



Global height-resolved methane retrievals from the Infrared Atmospheric Sounding Interferometer (IASI) on MetOp

Richard Siddans^{1,2}, Diane Knappett^{1,2}, Alison Waterfall¹, Jane Hurley¹, Barry Latter^{1,2}, Brian
5 Kerridge^{1,2}, Hartmut Boesch^{2,3}, Robert Parker^{2,3}

¹ STFC Rutherford Appleton Laboratory, Chilton, United Kingdom

² National Centre for Earth Observation, United Kingdom

³ University of Leicester, United Kingdom

Correspondence to: R. Siddans (richard.siddans@stfc.ac.uk)

10 **Abstract.** This paper describes the global height-resolved methane (CH₄) retrieval scheme for the Infrared Atmospheric
Sounding Interferometer (IASI) on MetOp, developed at the Rutherford Appleton Laboratory (RAL). The scheme is novel
in: (a) precisely fitting measured spectra in the 7.9 micron region to allow information to be retrieved on two independent
layers centred in the upper and lower troposphere and (b) making specific use of nitrous oxide (N₂O) spectral features in the
15 same spectral interval to directly retrieve effective cloud parameters to mitigate errors in retrieved methane due to residual
cloud and other geophysical variables. The scheme has been applied to analyse IASI measurements between 2007 and 2015.
Results are compared to model fields from the MACC greenhouse gas inversion and independent measurements from
satellite (GOSAT), airborne (HIPPO) and ground (TCCON) sensors. The scheme is shown to be capable of retrieving
column average methane with random errors of ~20-40 ppbv on individual soundings. Systematic differences with the other
20 datasets are typically < 10 ppbv regionally, and < 5 ppbv globally. The data has been made publically available via CEDA
(<http://dx.doi.org/10.5285/B6A84C73-89F3-48EC-AEE3-592FEF634E9B>).

1 Introduction

Methane (CH₄) is one of the most important long-lived greenhouse gases in the atmosphere. Its concentration in the
troposphere has increased by a factor of around 2.5 since pre-industrial times, mainly as a result of human activity (IPCC
25 2013). Currently, natural and anthropogenic sources have similar global annual magnitudes. The largest sources are from
fossil fuel extraction/use, ruminant livestock, decomposition of waste, rice cultivation (all anthropogenic), wetland
emissions, geological sources, termites (natural) and biomass burning (both anthropogenic and natural). Current emission
estimates are subject to considerable uncertainties (IPCC 2013, Kirschke 2013), and prediction into the future is even more
uncertain. Large amounts of methane are stored in Arctic permafrost and clathrates on the ocean floor: methane release from
30 these stores, as a result of warming, would lead to a strong positive feedback on climate.



The atmospheric abundance of methane is determined by surface emissions, balanced by chemical sinks; predominantly via reaction with hydroxyl radical. Between 1999 and 2006 there was little growth in the annually-averaged global methane concentration, but since then a significant increase of around 5 ppbv per year has been observed at surface level (Rigby 2008, Sussman 2012). The reasons for this recent behaviour are not yet clear (Nisbet 2014).

5 Global observations from nadir-viewing satellite sensors can now provide information to complement and extend that available from surface *in-situ* and remote-sensing measurements to improve our knowledge of the processes controlling the atmospheric distribution of methane, and to monitor its variability on a decadal scale. Methane can be measured remotely using bands in the shortwave infra-red (SWIR) and thermal infra-red (TIR). Observations in the SWIR, such as those from Envisat-SCIAMACHY (Buchwitz 2005, Frankenberg 2010) and GOSAT-TANSO-FTS (Butz 2010, Parker 2011 and

10 Yoshida 2013) provide information on column average methane with a vertical sensitivity, in cloud-free conditions over most land surfaces, which is close to uniform throughout the atmospheric column. Such measurements rely on surface-reflected sunlight, so observations are limited to daytime and predominantly over land (ocean reflectance being too low except in sun-glint geometry). TIR measurements of methane are available from spectrometers including Aura-TES (Worden 2012) Aqua-AIRS (Xiong 2008) and MetOp-IASI (Razavi 2009, Crevoisier 2013, Xiong 2013). These complement the

15 SWIR observations in regard to both vertical-sensitivity and geographical/temporal coverage. Because TIR spectral signatures depend on thermal contrast between the atmosphere and surface, sensitivity tends to be strong in the mid to upper troposphere and relatively low near the surface. TIR measurements are made over both land and sea, and during day and night. The spatial sampling of IASI is also much greater than that of GOSAT (the only currently operating SWIR methane sensor following the loss of Envisat in 2012): IASI provides 1.3 million soundings per day (with 12 km diameter footprint at nadir), over a sufficiently wide swath to provide approximately even sampling of all longitudes (Clerbaux 2009, Eumetsat 2014). IASI is currently flying on both MetOp-A (since 2006) and -B (since 2012); effectively doubling the spatial sampling. Eumetsat plans MetOp-C to take over from -A around 2018, to be followed by IASI Next Generation on the MetOp 2nd generation series from 2022-2040; yielding a self-consistent global data set from 2007 onwards. In contrast, GOSAT typically provides of order 1000 soundings per day (10.5 km diameter footprint), over a relatively narrow swath about the 14

25 ground tracks (Kuze 2016, Crisp 2012).] The potential for TIR and SWIR observations to be used together to infer near-surface methane concentrations is studied in (Worden 2015).

This paper describes the global height-resolved methane retrieval scheme developed at the Rutherford Appleton Laboratory (RAL). Novel aspects of the scheme include:

- Fitting measured spectra in the 1232-1288 cm^{-1} interval to typically ~ 0.1 K root mean square (RMS) precision, allowing information to be retrieved on two independent height layers centred in the upper and lower troposphere.
- Sophisticated use of nitrous oxide (N_2O) spectral features in the same interval to estimate effective cloud parameters which mitigate errors in retrieved methane due to residual cloud and other geophysical variables affecting radiative transfer. Although existing schemes (Razavi 2009, Worden 2012) make use of the fact that N_2O



retrievals from the same spectral range as CH₄ are affected similarly by errors such as residual cloud contamination and temperature errors, their approaches jointly retrieve methane and N₂O and correct methane *post-hoc*, based on the difference between retrieved N₂O and its assumed distribution, relying on the fact that tropospheric N₂O is very close to being uniformly mixed throughout the troposphere with a mixing ratio known to a high degree of accuracy.

5 In the scheme described here, we explicitly model the N₂O vertical profile spanning the stratosphere, where it varies strongly with height, latitude and season, as well as the troposphere, where it is specified to be uniformly-mixed. The N₂O spectral signature is instead used to co-retrieve an effective cloud-fraction and height for the fit window, yielding a physically-consistent and more accurate retrieval of methane. An important consequence of modelling the cloud effect directly, compared to the *post-hoc* correction approach using co-retrieved N₂O, is that the effect of

10 cloud on the vertical sensitivity of the retrieved CH₄ is included in the resulting averaging kernels. We also note that joint retrieval of cloud with trace gases is a fundamental part of the TES algorithm described by Kulawik 2006 and Eldering 2008, however this uses a much wider spectral range (8-15 microns). The specific use of N₂O absorption lines within the relatively narrow methane fit range, coupled to sophisticated modelling of the N₂O stratospheric distribution, is key to ensuring that the simplistic representation of cloud in the retrieval is able to effectively

15 represent the impact of cloud on the CH₄ signal.

2 Data Processing Scheme

2.1 Optimal Estimation

The scheme is based on the optimal estimation method (OEM, Rodgers 2000), which solves an otherwise under-constrained inverse problem by introducing prior information. This method finds the optimal state-vector \mathbf{x} (which contains the

20 parameters we wish to retrieve) by minimising a cost function:

$$\chi^2 = (\mathbf{y} - F(\mathbf{x}))^T \mathbf{S}_y^{-1} (\mathbf{y} - F(\mathbf{x})) + (\mathbf{a} - \mathbf{x})^T \mathbf{S}_a^{-1} (\mathbf{a} - \mathbf{x}), \quad (1)$$

where \mathbf{y} is a vector containing each IASI spectral brightness temperature measurement used by the retrieval; \mathbf{S}_y is a covariance matrix describing the errors on the measurements; $F(\mathbf{x})$ is the forward model (FM), which predicts measurements given \mathbf{x} ; \mathbf{S}_a is the *a priori* covariance matrix, which describes the assumed errors in the *a priori* estimate of the state, \mathbf{a} . As

25 the FM is non-linear with respect to perturbations in methane and other elements of the state-vector, the solution state needs to be found iteratively. In this case we adopt the well-known Levenburg-Marquardt method (summarised in Press 1995), assuming convergence to have occurred when the change in cost-function value is smaller than 1.

2.2 Measurements

IASI (Blumstein 2004) provides spectra at 0.5 cm⁻¹ apodised resolution, sampled every 0.25 cm⁻¹, from 625 to 2760 cm⁻¹.

30 Spectra are measured with 4 detectors, each with a circular field of view on the ground (at nadir) of approximately 12 km



diameter, arranged in a 2 x 2 grid within a 50 x 50 km field-of-regard (FOR). IASI scans to provide 30 FORs (120 individual spectra) evenly distributed across a 2200 km wide swath. Our retrieval scheme uses measurements between 1232.25 and 1288.00 cm^{-1} , chosen following the work of Razavi (2009) to: (a) minimise errors caused by neglecting line-mixing in the forward model and (b) include channels with relatively clear transmission to the ground, to help constrain co-retrieved cloud parameters and surface temperature. Channels between 1245-1246.75 cm^{-1} and 1267-1270 cm^{-1} are omitted to avoid problematic spectral features (in the former range attributed to line-mixing effects).

The noise on individual IASI spectra is particularly low in this spectral range (Hilton 2012), with noise-equivalent brightness temperature (NEBT) around 0.07 K (for a reference scene temperature of 280 K), corresponding to a noise equivalent spectral radiance (NESR) of 5.8 $\text{nW}/\text{cm}^2/\text{cm}^{-1}/\text{sr}$. Early retrievals from this range revealed a significant contribution from scene photon noise, so we adopt the following in-house model of the estimated error in each channel:

$$\Delta y_{noise} = \sqrt{h + o \bar{I}}, \quad (2)$$

where parameters o and h are constants derived empirically from an analysis of the random component of fit residuals in this range (from an early version of the retrieval scheme) and \bar{I} is the mean spectral radiance over the complete IASI band. This yields NESR values ranging from 3 to 10 $\text{nW}/\text{cm}^2/\text{cm}^{-1}/\text{sr}$ over the typical range of band-averaged measured radiances.

2.3 Forward model

RTTOV version 10 (Matricardi 2009) is the basis of the RAL FM. RTTOV estimates radiances convolved with the IASI spectral response function by use of spectrally-averaged layer transmittances, based on a fixed set of coefficients which weight atmospheric-state-dependent predictors. The RTTOV v10 model is sufficiently fast to enable global processing of the IASI mission with modest computational resources. In order to allow interference from the water vapour isotopologue HDO to be modelled adequately, this is handled as an independent variable to the major isotopologue H_2^{16}O . We have derived coefficients specifically for this spectral range, by running the line-by-line Reference Forward Model (RFM) (Dudhia 2016) using HITRAN 2008 (Rothman 2009) spectroscopic line data for the same set of atmospheric profiles and predictors used in (Matricardi 2009), with the exception that predictors of the type used for CO are used instead to predict HDO transmittances. The accuracy of the RTTOV model with the new HDO coefficients is tested by comparing radiances from RTTOV to those calculated directly with the RFM for an independent set of atmospheric profiles. The mean and standard deviation of these differences are generally found to be <0.05 K, though standard deviations can exceed 0.2 K in a few spectral channels particularly where water vapour transmittances are comparable to those of another variable gas. This source of forward model error is accounted for in the retrieval by adding the RTTOV-RFM variances to the diagonals of the IASI measurement error covariance matrix (S_y).



The ECMWF ERA-Interim (Dee, 2011) re-analysis is used to define the atmospheric temperature profile and the surface pressure appropriate for each IASI scene. Re-analysis fields are provided at 6 hourly intervals, approximately 0.7 degrees horizontal resolution, on 60 vertical levels. These fields are linearly interpolated to the IASI location and time. Profiles of methane and water vapour (including the isotopologue HDO) are defined by the retrieval state vector (see below), as is the surface (skin) temperature.

A fundamental distinguishing feature of the RAL scheme is the sophisticated approach developed to specify the N₂O vertical profile at each IASI measurement location for use in the FM. N₂O is modelled so that its spectral features can be exploited to co-retrieve two effective cloud parameters, and thereby mitigate related errors on the retrieved methane. In the troposphere, N₂O exhibits variations with latitude and season smaller than ~0.5% (IPP, 2013); approximately an order of magnitude smaller than those of methane. The annual growth rate of N₂O since IASI became operational in 2007 (around 0.23%/year) has been much more consistent than that of methane in recent decades. Mixing ratios of both N₂O and methane decrease with height in the stratosphere. In the case of N₂O, the decrease commences at lower altitude and is steeper than for methane¹. It is therefore particularly important to accurately model the stratospheric N₂O profile pertaining to individual IASI observations. The lifetime of N₂O in the stratosphere is such that spatial and day-to-day variability is controlled by dynamics, and can therefore be modelled accurately by exploiting the strong correlation, on potential temperature surfaces, between N₂O and potential vorticity. This is implemented in the RAL scheme using the seasonal N₂O climatology derived from the ACE-FTS solar occultation sensor (Jones 2012) which is expressed as a function of equivalent latitude (Lary 1995) and pressure. This is filled below the tropopause with a fixed mixing ratio of 322 ppbv, a representative value for the global mean at the beginning of 2009. The zonal mean field is linearly interpolated to the day of year of a given IASI observation. The N₂O vertical profile at the locations of individual IASI observations is estimated using the local equivalent latitude, derived from potential vorticity and potential temperature given by the ERA-interim re-analysis. The long-term, monotonic growth rate in N₂O is modelled by scaling each derived profile by the factor: $f = 1 + 0.0023d$, where d is the number of elapsed days since the beginning of 2009.

Over sea, the RTTOV sea surface emissivity model is used. Over land, the retrieval currently uses the University of Wisconsin surface emissivity database (Seeman 2008). Principal components of an ensemble of measured land surface spectral emissivity spectra are used in conjunction with 0.1 degree latitude/longitude gridded monthly data from MODIS to generate global maps of spectral resolved emissivity.

It is found that fits to measured spectra based on this FM lead to residuals (i.e. differences between observed and modelled spectra) which are small (<0.5 K RMS) but still significant compared to the IASI NEBT (see section 2.2). Column average mixing ratios from retrieved methane profiles are positively biased compared to independent measurements by approximately 4%, with a systematic height-dependent structure in the profile. A similar bias has been found in TES retrievals which exploit the same spectral range (Worden 2012) and also in MIPAS stratospheric retrievals in limb geometry

¹ In the case of N₂O the decrease with height is due to UV photolysis whereas for methane (CH₄) it is due to reaction with O(¹D).



(Von Clarmann 2009), suggesting a cause related to spectroscopic line parameters. To assess this, retrievals have been carried out substituting RTTOV with the RFM and LBLRTM line-by-line model, with both Hitran 2008 and 2012 line data. LBLRTM includes an approximate treatment of line mixing (Alvaredo 2013). None of these tests led to a significant reduction in the positive bias with respect to independent (TCCON) data. The following approach was therefore taken to empirically address these forward model related issues:

1. On input to RTTOV, all methane mixing ratios are multiplied by a factor 1.04 compared to the values in the state vector (i.e. the FM assumes 4% more methane than is ultimately reported as the retrieved value).
2. Spectral mean residual patterns derived from applying the retrieval scheme to one day of IASI data over cloud-free ocean in the latitude range of 75° S to 15° S are adopted to represent the mean forward model error and its scan-angle dependence. In this version of the scheme, rather than retrieve a height-resolved profile, the methane profile shape is specified, using a similar approach to that adopted to define N₂O, and a single scale factor retrieved. The resulting mean residual spectrum from the nadir view, \mathbf{r}_0 , has negligible correlation with the spectral weighting function for the altitude-independent scaling of the methane profile. The scan-angle dependent component of the FM error is estimated as $\mathbf{r}_1 = \mathbf{r}_E - \mathbf{r}_0$, where \mathbf{r}_E is the mean residual from both outer edges of the swath.
3. To retrieve global methane retrievals, a version of the FM which accounts for the spectral mean residual by adjusting the measurement vector as:

$$\mathbf{y} = \mathbf{y}_{RTTOV} + f_0 \mathbf{r}_0 + f_1 \mathbf{r}_1, \quad (3)$$

where \mathbf{y}_{RTTOV} is the radiance vector predicted by RTTOV and factors f_0 and f_1 are co-retrieved with methane and other parameters in the state vector, on a scene-by-scene basis.

It is noted that spatial variations in retrieved values of f_0 suggest that the mean residual features are at least partly related to the water vapour distribution.

2.4 Selection of IASI observations for processing

The brightness temperature (BT) difference between the IASI observation in a window channel (950 cm⁻¹) and that simulated on the basis of ERA-interim, assuming clear-sky conditions, is used to screen out scenes which are strongly affected by cloud. If this difference (observation – simulation) is outside the range of -5 to 15 K, the scene is not processed. Furthermore, only scenes having a BT larger than 240 K in the same channel are currently processed, since (a) the retrieval information content is significantly degraded over very cold surfaces (see below) and (b) convergence is often found to be slow in these conditions, leading to a disproportionate use of computational effort.

The IASI MetOp-A orbits from 29 May 2007 to 17 November 2015 have all been processed with this approach, selecting from the four pixels in each field-of-regard the IASI pixel with the warmest BT at 950 cm⁻¹.



2.5 State vector and *a priori* constraint

The state vector for the retrieval scheme consists of 34 elements, as follows:

- Methane mixing ratio (in ppmv, relative to dry air) defined on 12 fixed pressure levels corresponding to z^* values of 0, 6, 12, 16, 20, 24, 28, 32, 36, 40, 50, 60 km, where z^* is a simple transformation of pressure, p , (in hPa) to approximate geometric altitude (km):

$$z^* = 16(3 - \log_{10} p) , \quad (4)$$

The *prior* state is defined to be a fixed value of 1.75 ppmv in the troposphere, broadly representative of southern hemisphere mid-latitudes in 2009, and an annual average height-latitude cross-section in the stratosphere. The zonal mean is calculated by averaging into 5 degree latitude bins two years (September 2008-10) of output from the TOMCAT chemical transport model run into which ACE-FTS observations of long-lived stratospheric tracers have been assimilated (Chipperfield 2002). *A priori* errors are estimated as the root-mean-square combination of the standard deviation of the model methane field about its zonal mean and 10% of the *a priori* value itself. The model standard deviations in the troposphere are around 5%, so *a priori* errors in the troposphere are set to 175 ppb (i.e. 10% of the *prior* value), increasing (in fractional terms) above the tropopause up to peak values of around 50%. The *prior* state and errors are interpolated in latitude to the location of a given IASI observation. To help regularise the retrieval, off-diagonal elements are defined assuming a Gaussian function in the vertical with full-width half-maximum 6 km (in z^* units). Here we make a deliberate choice to define a simple and relatively weak constraint to emphasise the vertical resolved information in the IASI measurements. A tighter constraint, which could be justified based on climatological variability, is not necessary to regularise the retrieval and would increase the bias towards the prior (already evident towards high latitudes from the evaluation reported below).

- Natural logarithm of the water vapour (H_2O) mixing ratio (in ppmv) defined on 16 fixed pressure levels corresponding to z^* values of 0, 1, 2, 3, 4, 5, 6, 8, 10, 12, 16, 20, 30, 40, 50, 60 km. The *a priori* profiles for water vapour are taken from ECMWF analysis, interpolated (linearly) onto these pressure levels. The *a priori* error covariance is intended to represent (conservatively) errors in the analysis and those associated with interpolation to the time and location of an individual IASI observation:

$$\mathbf{S}_{a:H_2O} = \mathbf{S}_{bg} + \mathbf{S}_{dt} + \mathbf{S}_{dx} , \quad (5)$$

where \mathbf{S}_{bg} is the ECMWF model background error covariance matrix taken from (Collard 2007); \mathbf{S}_{dt} is the covariance of differences (considering all profiles in a given day) between ECMWF profiles at one of the 6 hourly analysis times and those at the next analysis time; \mathbf{S}_{dx} is the analogous covariance of differences between neighbouring spatial grid points. This results in a covariance matrix with relatively large diagonal elements



(corresponding to standard deviations of up to 60% peaking in the mid-troposphere), but sufficient vertical correlation to regularise the retrieval.

- Scale factor for HDO, with *a priori* value of 1 and assumed *prior* error of 1. This defines the HDO profile assumed in the FM as follows:

$$r_{HDO}(p) = f_{HDO} f_{std} r_{H_2O}(p), \quad (6)$$

where f_{HDO} is the retrieved factor; f_{std} is the (fixed) ratio of HDO:H₂¹⁶O assumed by HITRAN (3.107×10^{-4}) and $r_{H_2O}(p)$ is the (retrieved) water vapour main isotope mixing ratio profile.

- Natural logarithm of the (effective) cloud fraction and the associated cloud pressure (hPa). Cloud is modelled in RTTOV as a black body at the given atmospheric level, occupying a given geometric fraction of the scene. The *a priori* cloud fraction is assumed to be 0.01 (before converting to log) and the *a priori* error is assumed to be 10 (which, given the log representation, is a fractional error of 1000% with respect to the prior value of 0.01). The *a priori* cloud pressure is 500 hPa, with error 500 hPa. The logarithm is used as it is found to lead to more stable convergence (non-physical states with negative cloud fraction can otherwise arise during the cost-function minimisation).
- Surface temperature, with *a priori* value taken from ECMWF analysis and assumed *a priori* error of 5 K.
- The two scale factors for systematic residuals. *A priori* values are 1 for f_0 and 0 for f_1 . Both are assigned an *a priori* error of 1.

Results from this retrieval scheme are compared below to an earlier version of the scheme, which is identical except that (i) the two cloud parameters are *not* retrieved (scenes passing the initial cloud test are assumed cloud-free) and (ii) the N₂O profile is jointly retrieved, rather than being modelled. The N₂O prior state and errors are defined in the same way as methane, except that the profiles are scaled, by the same factor at all altitudes, to give a peak mixing ratio in the troposphere of 0.319 ppmv.

3 Error analysis and retrieval characterisation

The error covariance of the solution from an optimal estimation retrieval is given by:

$$\mathbf{S}_x = (\mathbf{S}_a^{-1} + \mathbf{K}^T \mathbf{S}_y^{-1} \mathbf{K})^{-1}, \quad (7)$$

where \mathbf{K} is the weighting function matrix which contains the derivatives of the FM with respect to each element of the (solution) state vector. The square-roots of the diagonal elements of this matrix are referred to as the *estimated standard deviation* (ESD) of each element of the state vector.



The transformation from the retrieved methane mixing ratio profile, \mathbf{x} , to the dry-air column averaged mole fraction, c , is expressed as a matrix operation $c = \mathbf{M}\mathbf{x}$, where \mathbf{M} contains the weights required to perform the linear operations (i) interpolate the profile defined on the state vector grid to the finer grid used in the radiative transfer model (ii) integrate to give the total column amount (iii) normalise by the total column of air. The ESD of the column average is then given by

$$5 \quad \Delta c = \sqrt{\mathbf{M} \mathbf{S}_x \mathbf{M}^T}. \quad (8)$$

The sensitivity of the retrieval to perturbations in the measurement is given by the gain matrix, $\mathbf{G} = \mathbf{S}_x \mathbf{K}^T \mathbf{S}_y^{-1}$. The sensitivity of the retrieval to perturbations in the true state vector is characterised by the averaging kernel, $\mathbf{A} = \mathbf{G}\mathbf{K}$.

\mathbf{S}_x can be divided into two terms:

$$10 \quad \mathbf{S}_x = \mathbf{S}_n + \mathbf{S}_s, \quad (9)$$

where $\mathbf{S}_n = \mathbf{G} \mathbf{S}_y \mathbf{G}^T$ describes the uncertainty due to measurement errors (characterised by \mathbf{S}_y) and $\mathbf{S}_s = (\mathbf{I} - \mathbf{A})\mathbf{S}_a(\mathbf{I} - \mathbf{A})^t$ describes the smoothing error, i.e. departure from the true state caused by the tendency of the retrieval towards the imposed *a priori* constraint. As discussed in von Clarrman (2013), the smoothing error only applies to the profile as represented on the (rather coarse) retrieval grid. A consequence of this is that the ESD of the total column from equation 8 does not fully capture errors arising from the insensitivity of the retrieval to fine scale perturbations in the vertical profile. Since methane is well-mixed in the troposphere, this issue will often be of little consequence, although there will be a tendency to underestimate total column errors (as well as the column itself) in the vicinity of strong sources where relatively high methane concentrations are present close to the ground. Vertical smoothing errors will be generally overestimated as the *prior* uncertainty on methane exceeds its natural variability. However, the ESD computed in this way corresponds well to the RMS difference between individual IASI measurements and independent TCCON data (see below).

Issues relating to the sensitivity of the retrieval to vertical structure and smoothing errors can be addressed using the fine-scale averaging kernel:

$$\mathbf{A}_f = \mathbf{G}\mathbf{K}_f \quad (10)$$

25 The weighting function \mathbf{K}_f is distinguished from \mathbf{K} in that derivatives may be computed with respect to perturbations on a finer grid than that used for the state vector. The averaging kernel for the sub-column average is $\mathbf{A}_{cf} = \mathbf{M}\mathbf{A}_f$.

The trace of the averaging kernel \mathbf{A} , evaluated using the weighting functions with respect to the retrieved state ($\mathbf{A} = \mathbf{G}\mathbf{K}$), gives the degrees of freedom for signal (DOFS), which indicates the number of independent pieces of information which can be recovered from the retrieval.

30 Figure 1 shows averaging kernels for methane, typical of mid-latitude, for nadir observing conditions. The surface temperature is assumed equal to the temperature of the lowest atmospheric layer. The panel on the left shows results assuming an NEBT at 280 K of 0.5 K, while that on the right shows results for 0.1 K (commensurate with the actual IASI



noise). Fitting close to this level is shown to be very important, adding 0.9 DOFS, and increasing sensitivity to lower tropospheric methane.

The gain matrix can also be used to estimate the impact of errors not characterised in the measurement or *prior* covariance, e.g. given the covariance of errors in the temperature profile \mathbf{S}_T , the resulting covariance of errors in the retrieved state is:

5

$$\mathbf{S}_{x:T} = \mathbf{G}\mathbf{K}_T\mathbf{S}_T(\mathbf{G}\mathbf{K}_T)^t, \quad (11)$$

where \mathbf{K}_T contains the derivatives of the FM with respect to temperature (defined on the same arbitrarily fine vertical grid as \mathbf{S}_T).

- 10 Figure 2 shows estimated error contributions to the retrieved methane profile and derived column averages (for the same assumptions as the right hand panel in figure 1). The plot shows ESD, noise and smoothing errors. It also shows three estimates of temperature errors, applying equation 11, to three different temperature error covariance matrices, each expressed on the model levels of the ECMWF analysis used: (i) “*background*” - the ECMWF forecast background error covariance matrix, from Collard (2007); (ii) “*sampling*” - an estimate of the error associated with interpolating ECMWF
- 15 temperature profiles to the times and locations of IASI soundings, determined in the same way as for water vapour (terms $\mathbf{S}_{dt} + \mathbf{S}_{dx}$ in equation 5); (iii) “*IASI*” - an error covariance matrix estimated for results from the (version 6) Eumetsat operational IASI temperature retrieval. The plot shows the ESD for column averaged mixing ratio is 28 ppbv and the error from modelling temperature is of comparable magnitude. In principle, these errors could be mitigated using temperature profiles retrieved from IASI itself².
- 20 The sensitivity of the retrieval is dependent on meteorological conditions (particularly the surface/atmospheric temperature profile and thermal contrast between atmosphere and surface). This is reflected in the geographical and seasonal variation in the column averaged ESD as summarised, using retrieval results in 2009 and 2010, in figure 3. Figure 4 illustrates the variation of the averaging kernel for the column averaging mixing ratio. Averages from IASI retrievals performed in January and July 2009 are shown in 10 degree latitude bands. In the figure, the two months are presented as *winter* and *summer*
- 25 conditions, with data for summer conditions taken from the January zonal mean in the southern hemisphere and the July mean in the north (vice-verse for the winter). Diurnal variations in surface temperature and air-ground thermal contrast cause the sensitivity of methane retrievals over land to differ between daytime (descending node, 9:30am local solar time) and night-time (ascending node, 9:30pm) observations. Methane retrievals over land generally show greater near-surface sensitivity in daytime than night-time. Due to thermal inertia of the ocean, methane retrieval performance is more uniform
- 30 with respect to latitude, season and time of day than it is over land. In summer, daytime sensitivity is greater over land than sea; however, the situation is reversed in the winter at mid-latitudes (when the sea is typically warmer than the land).

² A pre-retrieval of temperature and humidity profiles and surface spectral emissivity is in development.



The methane retrieval scheme is influenced by the specified N_2O distribution. Simulations for cloud-free conditions show that over a realistic range of N_2O perturbations, the methane retrieval responds linearly, such that a 1% height independent scaling of the N_2O profile gives rise to a similar magnitude error in retrieved column average methane. This arises because the co-retrieved cloud parameters accommodate the spectral signature of the N_2O error, and the retrieved methane profile then accommodates the impact of the erroneous cloud parameters on the methane spectral features. Although the retrieval scheme specifies a fixed tropospheric value of N_2O , the NOAA flask record indicates there to be a meridional gradient from the most southerly to northerly sites of order $\pm 0.5\%$ (IPCC). This would be expected to give rise to similar systematic errors in methane (± 10 ppb). Given the simple response of the retrieval to perturbing the assumed N_2O , it is possible to correct retrieved column average methane post-hoc, given a better estimation of the N_2O height-resolved distribution than that assumed in the retrieval (e.g. from a model), although such corrections have not been carried out in the analysis reported here.

4 Performance in the presence of cloud

The performance of the retrieval scheme in the presence of cloud depends on the ability of the two cloud parameters included in the fit to accommodate the real effects of cloud vertical and horizontal structure. The potential of the approach was initially demonstrated via retrieval simulations in which cloud optical properties and 3D structure on finer scales than the IASI field-of-view was explicitly represented in synthesizing measured spectra (Kerridge, 2012). In this paper, the impact of cloud on methane retrievals is confirmed using real IASI flight data. Differences between column average methane retrieved from IASI and those from the Total Column Carbon Observing Network (TCCON, see section 5.3) are examined as a function of cloud height and optical depth. For this purpose, effective cloud optical depth and height for each IASI measurement were estimated by applying the Optimal Retrieval of Aerosol and Cloud (ORAC) scheme (Poulsen, 2012) to co-located visible/near-IR and thermal-IR images observed by AVHRR/3 on-board MetOp. The ORAC scheme was applied to AVHRR/3 radiances averaged over each IASI field-of-view (given in the IASI Level 1 (L1) files) to give an effective³ optical depth and cloud height, together with phase and effective radius. Thick, high cloud is excluded from this analysis by the pre-selection of IASI measurements based on the BT difference test described earlier. All IASI retrievals within 100 km and 1 hour of all available TCCON measurements in 2009 were selected. The difference between all these IASI retrievals and the associated TCCON measurements were averaged into bins of the AVHRR/3-derived cloud optical depth and height (without attempting to correct for differences in vertical sensitivity). Results are summarised in Figure 5, for both our original scheme (N_2O retrieved, cloud neglected) and the current scheme (N_2O specified, cloud parameters fitted). Cloud leads to a strong positive bias in the methane retrieved by the original scheme. Figure 5 shows that, even though

³ Effective in the sense that cloud is here assumed to be homogenous both horizontally across the IASI field-of-view, and is represented by a geometrically thin single layer of either liquid or ice particles.



independent, co-located AVHRR/3-derived cloud information is potentially available⁴, the sensitivity of the original scheme to residual cloud is such that a very stringent filter would have to be applied to avoid significant error in IASI-retrieved column average methane. In practice, this would result in the vast majority of scenes having to be excluded. On the other hand, the scheme which co-retrieves two cloud parameters is shown to be much less sensitive to residual cloud: for cloud effective heights below 5 km, the methane retrieval has a bias of less than 30 ppbv. For cloud effective optical depth below 1, it is insensitive to cloud at all heights. The errors with respect to TCCON tend to be negative, especially for low altitude cloud of effective optical depth >3. As evident from the figure, co-retrieved cloud fraction (from the methane retrieval scheme) can be used in post-screening to remove methane retrievals which are likely to be biased, such that the vast majority of screened retrievals have a bias smaller than 5 ppbv. Results presented in the evaluation section below are based on using retrievals with an effective cloud fraction < 0.2.

5 Evaluation of the retrievals

5.1 Comparisons to MACC-II Greenhouse gas inversions

The MACC-II Greenhouse-gas (GHG) flux inversions provide global methane analyses based on the assimilation of measurements into the TM5 chemical-transport model (Bergamaschi, 2013). Daily average methane distributions are provided at a horizontal resolution of 6 degrees longitude by 4 degrees latitude. Here we focus on the re-analysis dataset (“v10-S1NOAA_ra”) which spans 2000-2012, based on the assimilation of NOAA surface level flask measurements. Column averaged methane and sub-column averages between pressure levels corresponding to $z^*=6$ and 12 km are considered. *Direct* comparisons with IASI are made by interpolating MACC-II GHG data for a given day to the geographical locations of individual IASI observations and averaging both into 2.5 x 2.5 degree longitude/latitude bins for individual months. As well as performing a simple comparison of column- and sub-column averages, we also account for *prior* influence and vertical sensitivity of the IASI retrieval using the averaging kernels as follows:

$$c_{Mxl} = c_a + \mathbf{A}_M(\mathbf{x}_M - \mathbf{a}_M), \quad (12)$$

where c_a is the column average computed from the *a priori* profile; \mathbf{A}_M is the averaging kernel matrix for the (sub-)column amount, computed from the retrieval gain and spectral weighting functions evaluated on the MACC-II GHG vertical grid; \mathbf{x}_M is the MACC-II GHG mixing ratio profile for a given day (interpolated to the location of an individual IASI observation); \mathbf{a}_M is the *a priori* profile interpolated to the MACC-II GHG vertical grid.

Figure 6 shows seasonal mean distributions of the column averages from IASI and MACC-II GHG, based on data processed between June 2009 and May 2010, and averaged into 7.5 x 5 degree longitude/latitude bins over 3 month intervals⁵. IASI and

⁴ Cloud retrieval from the ORAC scheme is available only during daytime.

⁵ This grid-size is chosen to be appropriate for the comparisons to GOSAT as discussed in the following section.



MACC-II GHG exhibit broadly similar spatial distributions (e.g. north-south gradient) and seasonal variations (in particular features associated with emissions in southern Asia). IASI daytime observations over land show generally larger values than MACC-II GHG, particularly over regions associated with surface emissions. In the *direct* comparison, (MACC-II GHG – IASI) differences are seen to be comparatively large at high northern latitudes. These differences are much reduced in comparisons accounting for the averaging kernels (labelled “MxI – IASI” in the figure), indicating *prior* influence on the retrieval accounts for most of the discrepancy. IASI tends to be biased low at high northern latitudes because the *a priori* tropospheric mixing ratio is biased low at these latitudes and, due to low surface temperature, IASI spectra are less sensitive to methane variations than they are at lower latitudes. Such discrepancies are less apparent at high southern latitudes where the *a priori* tropospheric mixing ratio is in reasonable agreement with MACC-II GHG. Use of the averaging kernels also reduces differences between MACC-II GHG and IASI over source regions in Asia. However, IASI is lower than MACC-II GHG (by up to 40 ppbv) over Arabia/Iran and the Sahara. It is also consistently lower (by 10-20 ppbv) over some regions of the tropical oceans, especially in March-May. On the other hand, from September-February it is consistently higher in southern mid-latitudes by ~20 ppbv. This could be partly explained by a low bias of MACC-II GHG against TCCON in the southern hemisphere reported in Alexe (2015). In comparisons to TCCON and GOSAT, IASI is found to be biased high (see section 5.2 and 5.3), though by a considerably smaller amount.

There are regions over the tropical oceans in which IASI is lower than MACC-II GHG by ~20 ppb, especially in March-May. Similar patterns appear also in IASI-GOSAT comparisons. A low bias in IASI data could plausibly be explained by persistent low cloud cover (see section 4 above); however, the geographical pattern of the bias is not fully consistent with this explanation (a similar bias is not present in other regions of known persistent low cloud cover). The bias could also be explained by the presence of slightly higher than expected tropospheric N₂O mixing ratio in these areas, which might be supported by HIPPO observations (Kort, 2011).

Figure 7 compares the 6-12 km sub-column averages from IASI and MACC-II GHG. Distributions are dominated by outflow from the south-east Asian monsoon, captured quite consistently by IASI and MACC-II GHG. In *direct* comparisons, MACC values are generally 10-20 ppbv lower than IASI. When averaging kernels are applied, which capture the influence on the retrieved 6-12km layer average from the atmosphere above and below, agreement is generally improved. However, a discrepancy is then revealed at high northern latitude; particularly in spring when MACC-II GHG values are ~20 ppbv larger than IASI values. These differences must be related to differences in representing the stratospheric profile and its contribution to the 6-12 km sub-column, either in IASI or MACC-II GHG⁶.

The evolution in time of these comparisons has been studied by averaging the monthly-binned IASI and MACC values from 2.5 x 2.5 degree latitude/longitude intervals into the regions illustrated in figure 8. Over land, these regions correspond to those used in the TRANSCOM model intercomparison exercise (from Fraser, 2013, based on Gurney 2002). Time-series of the column averages in these regions are shown in figure 9. Each panel compares IASI with MACC-II GHG (direct and after

⁶ For MACC-II GHG, stratospheric 3-D structure is that specified by TM5 whereas, for IASI, it is an annual average zonal-mean cross-section from TOMCAT, from which there will be systematic, seasonally-dependent departures.



applying the averaging kernels). The caption in each panel gives the correlation coefficient (“r”), mean difference (“m”) and standard deviation of the differences (“s”) between IASI and MACC-II GHG. Panels are organised in order of average latitude from north to south. IASI and MACC-II GHG clearly agree well on the secular trend in methane over the eight-year period 2007-15, and seasonal cycles also agree well. As noted previously, averaging kernels have the most impact at high northern latitudes; significantly increasing correlation coefficients in that case. After accounting for the averaging kernels, correlation coefficients are all ≥ 0.85 . Mean differences are ≤ 10 ppbv, except in southern mid-latitudes where IASI values are ~ 20 ppbv higher than MACC-II GHG. Standard deviations of the monthly, regional mean values are typically ~ 3 ppbv (although these are somewhat larger at high northern latitudes). This is an order of magnitude lower than the typical ESD of ~ 30 ppbv for an individual IASI sounding, but large in comparison to the standard-error in the mean (since many thousands of individual IASI soundings contribute to each monthly regional mean).

Figure 10 shows the corresponding time-series for the 6-12 km z^* layer sub-column average. Seasonal patterns are quite different from those of the total column average in some regions. In particular, tropical regions have relatively weak seasonal cycles in this upper layer compared to the total column average, and this is captured by IASI in accordance with MACC-II GHG. As with the total column average, correlation coefficients are ~ 0.9 after accounting for averaging kernels. The Arctic region shows the largest differences, with a quite distinct seasonal cycle evident in IASI cf MACC (whether or not averaging kernels are applied).

5.2 Comparisons to GOSAT retrievals

In this section IASI column average methane retrievals are compared with those produced by the University of Leicester (Parker, 2015) from the GOSAT short-wave infra-red (SWIR) spectrometer, using the so-called “CO₂ proxy” technique⁷. Version 6 data, as produced for the ESA Greenhouse Gas CCI project (Buchwitz, 2015), are used here. The approach described in section 5.1 for MACC-II GHG is adapted here to account for the sparse spatial sampling of GOSAT, especially over the ocean where retrievals only exist in sun-glint geometry: the starting point is to obtain 2.5 degree x 2.5 degree longitude/latitude daily binned fields from GOSAT and IASI (daytime only retrievals). Monthly mean fields are then accumulated from these daily files. In the IASI case, geographical sampling for each given day is restricted to only those grid cells for which GOSAT data also exists. The resulting monthly means are then further averaged to 7.5 x 5 degree longitude/latitude resolution, over three month intervals. 7.5 degree longitude resolution is chosen to be just sufficient to eliminate gaps that would otherwise appear between GOSAT orbit tracks in the resulting plots. GOSAT provides only a column average, so it is not possible to apply IASI averaging kernels directly. As an alternative, we use MACC-II GHG

⁷ In this approach, the ratio of CH₄ to CO₂ column average mixing ratios is retrieved from a spectral interval around 1.6 microns containing both methane and CO₂ bands. The CH₄:CO₂ ratio is multiplied by the CO₂ column average from a model. The approach exploits the fact that CO₂ deviations from uniform mixing are much smaller than those of methane, and allows errors in instrument characterisation and radiative transfer modelling to largely cancel out.



vertical profiles to account for both GOSAT and IASI averaging kernels in comparing the two satellite sensors, and apply both to the IASI retrieval as follows⁸:

$$c_{I:G} = c_I + c_{MxG} - c_{MxI} , \quad (13)$$

where c_I is the IASI retrieved column average; c_{MxI} and c_{MxG} are the MACC column averages accounting for the IASI and GOSAT averaging kernels respectively, and $c_{I:G}$ is an estimate of what GOSAT is expected to observe, having adjusted the IASI retrieved column average to account for differences in vertical sensitivity of IASI and GOSAT.

Results are illustrated in figure 11. Differences between GOSAT and IASI are seen to be broadly similar to those found between MACC-II GHG and IASI (figure 6), which is consistent with the agreement found between the same GOSAT and MACC-II GHG data sets in Parker (2015). Adjusting for the different vertical sensitivities of IASI and GOSAT (using MACC-II GHG) is seen to account for most of the systematic difference between the two at high northern latitudes in winter and spring. The IASI values adjusted for vertical sensitivity are seen to be lower by 10-20 ppbv over Arabia, north Africa and over tropical oceans. At southern mid-latitudes IASI is higher (by ~10ppbv) than GOSAT. This bias is about a factor 2 smaller than that also seen in this region in the comparison to MACC-II GHG (from September-February), implying that MACC-II GHG is negatively biased with respect to both IASI and GOSAT in this region.

15 5.3 Comparison to TCCON

The Total Column Carbon Observing Network (TCCON) of ground-based Fourier transform spectrometers (Wunch, 2011) provides the most comprehensive set of ground-based total column methane measurements against which to validate satellite retrievals. Here we compare IASI to all available TCCON data from the latest release, version “GGG2014”. This includes data from the following sites: Armstrong Flight Research Center, Edwards (Iraci, 2014), Ascension Island (Feist, 2014), Bialystok (Deutscher, 2014), Bremen (Notholt, 2014), California Institute of Technology (Wennberg, 2014), Darwin (Griffith, 2014), Eureka (Strong, 2014), Four Corners (Dubey, 2014), Garmisch (Sussmann, 2014), Indianapolis (Iraci, 2014), Izana (Blumenstock, 2014), Jet Propulsion Laboratory (Wennberg, 2014a,b), Karlsruhe (Hase, 2014), Lamont (Wennberg, 2014), Lauder (Sherlock, 2014a,b), Manaus (Dubey, 2014), Orleans (Warneke, 2014), Paris (Te, 2014), Park Falls (Wennberg, 2014), Reunion Island (De Maziere, 2014), Rikubetsu (Morino, 2014), Saga (Shiomi, 2014), Sodankyla (Kivi, 2014), Tsukuba (Morino, 2014), and Wollongong (Griffith, 2014). For some stations, additional temporal coverage was given in the earlier GGG2012 release, and we exploit this here, using GGG2012 in periods when this is available but GGG2014 is not. Data for Ny Alesund was taken from the 2012 release. Locations of the TCCON stations used are indicated in figure 8.

⁸ Because GOSAT’s sensitivity varies little with height, unlike that of IASI, there is very little difference in practice between results using c_{MxG} in this equation or the uncorrected MACC-II GHG column average, c_M .



IASI column average data within 200 km of each TCCON station are averaged over a month for the days on which there are TCCON observations. Monthly averages are presented if there are at least one hundred IASI individual observations and ten TCCON observations contributing to each mean. Typically there are several thousand IASI observations contributing to each monthly mean, for which a standard error in the mean of ≤ 1 ppbv would be expected from typical ESDs on individual
5 retrieved column averages.

Since TCCON does not provide profile information, we cannot directly account for the effect of the IASI vertical sensitivity, but do so indirectly using MACC-II GHG as a transfer standard, as described for GOSAT comparisons in section 5.2. In order to extend this correction beyond the end of 2012, we use the MACC-II GHG delayed mode analysis (“v10_an”), which is available from 2013 until mid-2014. This assimilates GOSAT retrievals (from the RemoTec proxy scheme of Schepers
10 2012), in addition to the NOAA surface flask observations. The uniform height-sensitivity of direct-sun absorption measurements is such that the impact of the TCCON averaging kernel (on the monthly mean) is small compared to that of IASI, but is nevertheless taken into account in the adjusted “corrected” IASI estimate.

Time-series of comparisons to TCCON stations are shown in f12. In the absence of any TCCON measurements in a month, the IASI time-series is completed using the IASI monthly mean considering all days in the month (these points are shown for context/continuity in the plots but do not contribute to any derived statistics). As indicated in the panel headings, results from
15 some stations (seen to sample broadly similar methane variations) are grouped together to make the time-series in each panel more complete and to enable results to be presented in a more compact form.

The caption in each panel gives the correlation coefficient (r), mean difference (m) and standard deviation of individual TCCON-IASI differences (s); two values are given for each quantity (separated by “/”), corresponding to the direct
20 comparison of TCCON to IASI and the comparison to IASI after adjusting for vertical sensitivity (via MACC-II GHG profiles). Correlation coefficients before correction are 0.76 – 0.91 and generally improve after the adjustment. Correlation is only 0.65 (0.73 after correction) at Izana. Some of this degradation may be related to the high altitude of the station (2300 m) and/or its specific location (on Tenerife) which is subject to peculiar localised meteorological conditions and is in an area often affected by desert dust.

25 As might be expected, the correction generally raises the IASI values (as the tropospheric prior value is usually systematically low). The correction tends to have more impact in the north, although agreement with TCCON is not always improved. The correction usually reduces the standard deviation in the difference between IASI and TCCON. After correction, the mean difference and SD are ≤ 10 ppbv in most cases, with the notable exception of the Four Corners site. Here IASI captures the seasonal cycle well but underestimates TCCON by ~ 25 ppbv, even after correction. This anomaly is
30 presumably explained by the fact that the Four Corners TCCON site is located close to an extremely strong methane source associated with coal mining and related activities (Kort 2014), and so it samples localised methane variability not represented in IASI data sampled over a circular region of radius 200 km, nor by the MACC-II GHG data used in the adjustment.



Each panel in figure 12 also shows (as histograms along the x-axis, referring to the right-hand y-axis) the standard deviations (SDs) of IASI and TCCON data in monthly bins. Grey bars show the standard deviations of all individual IASI retrievals in each monthly bin. These are generally higher than those for TCCON (shown in light red), reflecting the significant contribution of random errors to individual IASI retrievals. These standard deviations are comparable to the ESD of individual retrievals, as computed by the optimal estimation retrieval scheme (illustrated in f3). The histogram indicated by the thin black line, shows for each given month the standard deviation of the set of the *daily mean* IASI values. Each daily mean is the average of all IASI observations within 200 km of the TCCON site. This quantity generally agrees rather well with the TCCON standard deviation, reflecting the day-to-day variation of methane within each month as seen by the two sensors. Again, the exception here is Four Corners, where TCCON has a higher standard deviation than IASI, supporting the hypothesis that this station samples methane variability which is substantial on a local scale.

Figure 13 summarises the TCCON comparisons for 2013 in a compact form, showing the individual monthly samples from TCCON and IASI as individual points, colour-coded by the site (or grouping of sites). Four Corners is excluded from this plot because of the sampling issue identified above. Error bars show the standard deviations of daily-mean values in each monthly bin. The top-left panel plots TCCON against the retrieval *prior*, whose variation arises from meridional structure in the annual mean stratospheric distribution. The absence of any discernible correlation between *prior* and TCCON values clearly demonstrates that agreement between the retrieval and TCCON to be wholly dependent upon information provided by the IASI measurements. It also illustrates why IASI retrievals tend to be biased low at high northern latitudes, where measurement sensitivity is lowest and the *prior* contribution is therefore most influential. The top centre panel shows the direct IASI/TCCON scatter which indicates a correlation coefficient of 0.92, and that IASI is systematically lower by ~11 ppbv. The top right panel shows the scatter between TCCON and the adjusted IASI retrieval, in which the correlation coefficient is increased to 0.95 and the negative IASI bias is reduced to ~1.5 ppbv. The standard deviation in the monthly IASI-TCCON differences is ~10 ppbv.

6 Comparison to HIPPO airborne observations

Aircraft *in-situ* measurements of methane profiles from HIAPER Pole-to-Pole Observations (HIPPO) provide an opportunity to compare with vertically-resolved satellite methane retrievals, e.g. see Wecht (2012), Alvaredo (2015). HIPPO executed five campaigns, each consisting of numerous individual flights, sampling over the US and Pacific between January 2009 and September 2011 (Wofsy, 2012). Methane profiles were measured *in situ* as the aircraft executed a series of ascent/descent manoeuvres. Most profiles sample only the mid/lower troposphere, though on occasions the manoeuvres extend into the upper troposphere. In order to make comparisons to column averages and sub-column averages, and to do so accounting for averaging kernels, we extend the HIPPO profiles by filling upwards with temporally and spatially interpolated profiles from the MACC-II GHG re-analysis.



We co-locate IASI and HIPPO data by selecting all IASI observations within 200 km and 6 hours of each individual HIPPO profile (taking the mean latitude, longitude and time of the aircraft measurement). We then compare each HIPPO profile to the mean of these IASI observations. The number of IASI samples in each mean profile is variable (typically in the range 1-20) due to cloud occurrence and latitude (more samples are found at high latitude where IASI's 2200km swaths overlap).

5 Figure 14 shows the comparison for HIPPO campaign 5, which is particularly interesting for our purposes as variations in the upper and lower tropospheric layers (represented here by 0-6 and 6-12 km sub-column averages) are quite distinct. These differences are very poorly captured by the IASI *prior*, but relatively well captured by the retrieval; illustrating that IASI can effectively resolve two independent layers centred in the lower and upper troposphere. There is a particularly pronounced meridional structure in the 6-12 km layer between profile index 30-40, which is captured by IASI and clearly present in both

10 HIPPO and the part of the field which has been infilled with MACC-II GHG data.

Figure 15 summarises (in a similar format analogous to figures of Alvarado,2015) the level of agreement between IASI and HIPPO, binning into 10 degree latitude intervals, the differences between the individual IASI/HIPPO matches, considering all five campaigns. The figure shows the mean difference (HIPPO-IASI) in each bin (with and without accounting for IASI averaging kernels), together with the standard deviation about the mean of the individual differences. For comparison, the

15 mean ESD of the IASI observations is also shown. The following points are evident: (1) After accounting for averaging kernels, the mean bias is -1.5 ppb (total column average), 3.7 ppb (0-6km layer average) and 0.24 ppb (6-12km layer average). As previously noted, accounting for averaging kernels, has most impact in the Northern hemisphere (where the prior methane is biased particularly low biased). (2) The standard deviation in the difference is similar whether or not averaging kernels are accounted for, and is almost always slightly smaller than the reported ESD. This is not surprising as

20 the ESD includes significant smoothing error, which will not manifest entirely as (quasi) random variability in the agreement betweenof IASI and HIPPO. (3) There is some latitude dependence in the bias, particularly in the lower tropospheric layer (still mainly within +/-20ppb). In particular, IASI seems to underestimate in the tropics. This behaviour is similar to that found between IASI and GOSAT column averages over the tropical oceans, as noted in section 5.2.

25 7 Summary and Conclusions

This paper reports a retrieval scheme for IASI developed at the Rutherford Appleton Laboratory (RAL) which, by fitting measured brightness temperature spectra in the 1232-1288 cm^{-1} interval to RMS precision of <0.1 K, is capable of extracting information on two independent layers centred in the upper and lower troposphere. Sensitivity near the surface depends upon thermal contrast with the surface and therefore the temperature structure of the lower atmosphere and surface conditions. A

30 novel feature of this scheme is to exploit the N_2O spectral band in the same window to co-retrieve an effective cloud fraction and height which substantially improves methane retrieval precision by mitigating the effects of residual cloud. The use of the RTTOV10 forward model makes the scheme sufficiently fast on the JASMIN-CEMS computer infrastructure at RAL to also run in near-real-time. The complete IASI MetOp-A record 2007-2015 has been processed, and this eight-year global



data set is publically available from the CEDA (<http://www.ceda.ac.uk/> , <http://dx.doi.org/10.5285/B6A84C73-89F3-48EC-AEE3-592FEF634E9B>).

The dataset has been extensively assessed by comparison to independent results from the MACC-II re-analysis based on greenhouse gas inversion and to correlative observations from the GOSAT satellite instrument, the TCCON surface network and pole-to-pole height-latitude transects from the HIPPO campaigns. Taken together, these comparisons indicate quasi-random errors of ~20-40 ppbv on individual IASI-retrieved column averages, in line with the estimated standard deviation (ESD) provided with each retrieval. After spatial and temporal averaging, and accounting for the vertical sensitivity of the IASI column average, systematic differences with the other datasets, are typically <10 ppbv regionally and <5 ppbv globally. The IASI retrieval is shown to capture the secular increase from 2007-2015 and seasonal variations of methane, yielding regional time series with correlations of typically 0.8-0.9 with respect to the MACC-II GHG inversion, in which surface fluxes were estimated from assimilation of NOAA flask measurements⁹.

It is important to take into account the sensitivity of the IASI retrievals, as characterised by the averaging kernels, and this is particularly the case at high latitudes. If not taken into account, IASI column averages appear negatively biased at high northern latitudes due to influence of the *prior* and systematically low *prior* value in the troposphere. Comparisons with MACC-II GHG and HIPPO, accounting correctly for vertical sensitivity, indicate IASI to be capable of resolving structures in the upper troposphere which are distinct from those in the lower troposphere; in line with our formal estimate of two degrees of freedom in the retrieved vertical profile.

This paper focuses on evaluation of the retrieval on relatively coarse spatial and temporal scales. IASI has a spatial resolution of 12 km, as determined by the fields-of-view of its individual detectors, and therefore has potential for resolving structure on that scale, including discrete emission sources. We note here that the current RAL scheme is limited at fine spatial scales by errors in representation of surface and atmospheric temperature (particularly in mountainous areas) and surface emissivity. These are expected to be mitigated significantly by using temperature and humidity profiles and surface spectral emissivity jointly pre-retrieved from IASI/MHS/AMSU¹⁰, which is being investigated in depth at present

Though it does not clearly emerge from the comparisons shown here, we note that users of the data should be cautious when using IASI methane retrievals in the presence of elevated sulphate aerosol, which is known to have significant spectral dependence in the 1232-1288 cm⁻¹ range used by this retrieval (Boer 2013, Clarisse 2013). Anomalies in methane retrievals have been noted which may be related to the eruptions of Sarychev in 2009 and Calbuco in 2015.

The scheme makes empirical corrections for discrepancies apparent between line-by-line modelled spectra and IASI observations. These discrepancies do not seem to be resolved by updates in HITRAN 2010, or the line-mixing approach used by LBLRTM. Further work is therefore needed to better understand the spectroscopy of methane and/or spectral interferents in this range.

⁹ After 2013, GOSAT column average data were assimilated in addition to NOAA flask data.

¹⁰ A new version of the methane retrieval scheme which works on this basis is at an advanced stage of development.



IASI also measures methane in the 3.7 micron spectral region. During the daytime, measurements in this range include a large surface-reflected solar contribution which contains information on near-surface methane which is complementary to that obtained from the 7.9 micron band. The potential to practically exploit this additional sensitivity is currently being investigated in depth.

- 5 This paper demonstrates that through IASI on MetOp-A and –B, as currently in orbit, and –C, due for launch in 2018/19, to be followed by IASI-NG on the MetOp-SG series 2020-40, the global, height-resolved methane distribution can be monitored over several decades to investigate variability caused by natural and anthropogenic emissions and composition-climate interactions.

10 Data availability

The IASI methane data described in this paper is publically available from the UK Centre for Environmental Data Analysis, CEDA (<http://www.ceda.ac.uk/>). The dataset can be reached via its digital object identifier (DOI): <http://dx.doi.org/10.5285/B6A84C73-89F3-48EC-AEE3-592FEF634E9B>.

15 Acknowledgements

This work has been funded by the UK Natural Environment Research Council (NERC) through the National Centre for Earth Observation (NCEO), and in part also by a Eumetsat study contract (contract no EUM/CO/14/4600001315/RM).

- 20 R. Parker and H. Boesch are funded by NCEO and ESA GHG-CCI, R.Parker is also funded by an ESA Living Planet Fellowship. We thank the Japanese Aerospace Exploration Agency, National Institute for Environmental Studies, and the Ministry of Environment for the GOSAT data and their continuous support as part of the Joint Research Agreement. This research used the ALICE High Performance Computing Facility at the University of Leicester.

- 25 Access to meteorological reanalysis data from ECMWF and IASI Level-1 data, along with JASMIN-CEMS computer infrastructure, has been provided by the Centre for Environmental Data Analysis at RAL.

TCCON data were obtained from the TCCON Data Archive, hosted by the Carbon Dioxide Information Analysis Center (CDIAC) – (<http://tccon.onrl.gov>).

- 30 HIPPO data was obtained from Carbon Dioxide Information Analysis Center (CDIAC) HIPPO Data Archive (<http://hippo.onrl.gov/>); DOI: http://dx.doi.org/10.3334/CDIAC/hippo_010.



MACC-II GHG Inversion data was obtained from the ECMWF: <http://apps.ecmwf.int/datasets/data/macc-ghg-inversions/>

GOSAT data used here has been provided by the ESA GHG CCI project (<http://www.esa-ghg-cci.org>).



References

- Alvarado, M. J., V. H. Payne, K. E. Cady-Pereira, J. D. Hegarty, S. S. Kulawik, K. J. Wecht, J. R. Worden, J. V. Pittman,
5 and S. C. Wofsy (2015), Impacts of updated spectroscopy on thermal infrared retrievals of methane evaluated with HIPPO
data, *Atmos. Meas. Tech.*, 8(2), 965–985, doi:10.5194/amt-8-965-2015.-
- Blumenstock, T., F. Hase, M. Schneider, O.E. García, E. Sepúlveda. 2014. TCCON data from Izana, Tenerife, Spain,
Release GGG2014R0. TCCON data archive, hosted by the Carbon Dioxide Information Analysis Center, Oak Ridge
10 National Laboratory, Oak Ridge, Tennessee, U.S.A. <http://dx.doi.org/10.14291/tcon.ggg2014.izana01.R0/1149295>
- Boera, Gregory J, Irina N. Sokolika, Scot T. Martin, Infrared optical constants of aqueous sulfate–nitrate–ammonium multi-
component tropospheric aerosols from attenuated total reflectance measurements—Part I: Results and analysis of spectral
absorbing features, *Journal of Quantitative Spectroscopy & Radiative Transfer* 108 (2007) 17–38
15
- Blumstein, D.; Chalon, G.; Carlier, T.; Buil, C.; Hébert, Ph.; Maciaszek, T.; Ponce, G.; Phulpin, T.; Tournier, B.; Siméoni,
D.; Astruc, P.; Clauss, A.; Kayal, G.; Jegou, R. (2004). "IASI instrument: technical overview and measured performances".
Proceedings of the SPIE. *Infrared Spaceborne Remote Sensing XII* 5543: 196–207. doi:10.1117/12.560907.
- 20 Buchwitz, M., R. de Beek, J. P. Burrows, H. Bovensmann, T. Warneke, J. Notholt, J. F. Meirink, A. P. H. Goede, P.
Bergamaschi, S. Korner, M. Heimann, and A. Schulz, Atmospheric methane and carbon dioxide from SCIAMACHY
satellite data: initial comparison with chemistry and transport models, *Atmos. Chem. Phys.*, 5, 941–962, 2005
- Buchwitz, M., M. Reuter, O. Schneising, H. Boesch, S. Guerlet, B. Dils, I. Aben, R. Armante, P. Bergamaschi, T.
25 Blumenstock, H. Bovensmann, D. Brunner, B. Buchmann, J. P. Burrows, A. Butz, A. Chédin, F. Chevallier, C. D.
Crevoisier, N. M. Deutscher, C. Frankenberg, F. Hase, O. P. Hasekamp, J. Heymann, T. Kaminski, A. Laeng, G.
Lichtenberg, M. De Mazière, S. Noël, J. Notholt, J. Orphal, C. Popp, R. Parker, M. Scholze, R. Sussmann, G. P. Stiller, T.
Warneke, C. Zehner, A. Bril, D. Crisp, D. W. T. Griffith, A. Kuze, C. O’Dell, S. Oshchepkov, V. Sherlock, H. Suto, P.
Wennberg, D. Wunch, T. Yokota, Y. Yoshida, The Greenhouse Gas Climate Change Initiative (GHG-CCI): comparison and
30 quality assessment of near-surface-sensitive satellite-derived CO₂ and CH₄ global data sets, *Remote Sensing of
Environment*, 162, 344–362, doi:10.1016/j.rse.2013.04.024, 2015.



- Butz, A., O. P. Hasekamp, C. Frankenberg, J. Vidot, and I. Aben, CH₄ retrievals from space-based solar backscatter measurements: Performance evaluation against simulated aerosol and cirrus loaded scenes, *JOURNAL OF GEOPHYSICAL RESEARCH*, VOL. 115, D24302, doi:10.1029/2010JD014514, 2010
- 5 Collard, A.D., Selection of IASI channels for use in numerical weather prediction, *Q. J. R. Meteorol. Soc.* 133: 1977–1991 (2007)
- Crevoisier, C., D. Nobileau, R. Armante, L. Crepeau, T. Machida, Y. Sawa, H. Matsueda, T. Schuck, T. Thonat, J. Pernin, N. A. Scott, and A. Chedin, The 2007–2011 evolution of tropical methane in the mid-troposphere as seen from space by
10 MetOp-A/IASI, *Atmos. Chem. Phys.*, 13, 4279–4289, 2013 www.atmos-chem-phys.net/13/4279/2013/ doi:10.5194/acp-13-4279-2013
- Crisp, D., B. M. Fisher, C. O’Dell, C. Frankenberg, R. Basilio, H. Bosch, L. R. Brown, R. Castano, B. Connor, N. M. Deutscher, A. Eldering, D. Griffith, M. Gunson, A. Kuze, L. Mandrake, J. McDuffie, J. Messerschmidt, C. E. Miller, I.
15 Morino, V. Natraj, J. Notholt, D. M. O’Brien, F. Oyafuso, I. Polonsky, J. Robinson, R. Salawitch, V. Sherlock, M. Smyth, H. Suto, T. E. Taylor, D. R. Thompson, P. O. Wennberg, D. Wunch, and Y. L. Yung, The ACOS CO₂ retrieval algorithm – Part II: Global XCO₂ data characterization, *Atmos. Meas. Tech.*, 5, 687–707, 2012, www.atmos-meas-tech.net/5/687/2012/, doi:10.5194/amt-5-687-2012
- 20 De Maziere, M., M. K. Sha, F. Desmet, C. Hermans, F. Scolas, N. Kumps, J.-M. Metzger, V. Dufлот, J.-P. Cammas. 2014. TCCON data from Reunion Island (La Reunion), France, Release GGG2014R0. TCCON data archive, hosted by the Carbon Dioxide Information Analysis Center, Oak Ridge National Laboratory, Oak Ridge, Tennessee, U.S.A. <http://dx.doi.org/10.14291/tcon.ggg2014.reunion01.R0/1149288>
- 25 Dee, D.P., S. M. Uppala, A. J. Simmons, P. Berrisford, P. Poli, S. Kobayashi, U. Andrae, M. A. Balmaseda, G. Balsamo, P. Bauer, P. Bechtold, A. C. M. Beljaars, L. van de Berg, J. Bidlot, N. Bormann, C. Delsol, R. Dragani, M. Fuentes, A. J. Geer, L. Haimberger, S. B. Healy, H. Hersbach, E. V. Holm, L. Isaksen, P. Kallberg, M. Köhler, M. Matricardi, A. P. McNally, B. M. Monge-Sanz, J.-J. Morcrette, B.-K. Park, C. Peubey, P. de Rosnay, C. Tavolato, J.-N. Thepaut and F. Vitart, The ERA-
30 Interim reanalysis: configuration and performance of the data assimilation system, *Q. J. R. Meteorol. Soc.* 137: 553–597, April 2011
- Deutscher, N., J. Notholt, J. Messerschmidt, C. Weinzierl, T. Warneke, C. Petri, P. Grupe, K. Katrynski. 2014. TCCON data from Bialystok, Poland, Release GGG2014R1. TCCON data archive, hosted by the Carbon Dioxide Information Analysis



Center, Oak Ridge National Laboratory, Oak Ridge, Tennessee, U.S.A.

<http://dx.doi.org/10.14291/tcon.ggg2014.bialystok01.R1/1183984>

Frankenberg, C., I. Aben, P. Bergamaschi, E. J. Dlugokencky, R. van Hees, S. Houweling, P. van der Meer, R. Snel, and P.
5 Tol, Global column averaged methane mixing ratios from 2003 to 2009 as derived from SCIAMACHY: Trends and
variability, JOURNAL OF GEOPHYSICAL RESEARCH, VOL. 116, D04302, doi:10.1029/2010JD014849, 2011, D04302
1

Dudhia, A. The Reference Forward Model (RFM). J. Quant. Spectrosc. Radiat. Transfer (2016),
<http://dx.doi.org/10.1016/j.jqsrt.2016.06.018>

10

Dubey, M., B. Henderson, D. Green, Z. Butterfield, G. Keppel-Aleks, N. Allen, J.-F. Blavier, C. Roehl, D. Wunch, R.
Lindenmaier. 2014. TCCON data from Manaus, Brazil, Release GGG2014R0. TCCON data archive, hosted by the Carbon
Dioxide Information Analysis Center, Oak Ridge National Laboratory, Oak Ridge, Tennessee, U.S.A.
<http://dx.doi.org/10.14291/tcon.ggg2014.manaus01.R0/1149274>

15

Dubey, M., R. Lindenmaier, B. Henderson, D. Green, N. Allen, C. Roehl, J.-F. Blavier, Z. Butterfield, S. Love, J.
Hamelmann, D. Wunch. 2014. TCCON data from Four Corners, NM, USA, Release GGG2014R0. TCCON data archive,
hosted by the Carbon Dioxide Information Analysis Center, Oak Ridge National Laboratory, Oak Ridge, Tennessee, U.S.A.
<http://dx.doi.org/10.14291/tcon.ggg2014.fourcorners01.R0/1149272>

20

Eldering, A., S. S. Kulawik, J. Worden, K. Bowman, and G. Osterman (2008), Implementation of cloud retrievals for TES
atmospheric retrievals: 2. Characterization of cloud top pressure and effective optical depth retrievals, J. Geophys. Res,
113(D16), D16S37, doi:10.1029/2007JD008858. Feist, D. G., S. G. Arnold, N. John, M. C. Geibel. 2014. TCCON data from
Ascension Island, Saint Helena, Ascension and Tristan da Cunha, Release GGG2014R0. TCCON data archive, hosted by the
25 Carbon Dioxide Information Analysis Center, Oak Ridge National Laboratory, Oak Ridge, Tennessee, U.S.A.
<http://dx.doi.org/10.14291/tcon.ggg2014.ascension01.R0/1149285>

[Fraser, A., P. I. Palmer, L. Feng, H. Boesch, A. Cogan, R. Parker, E. J. Dlugokencky, P. J. Fraser, P. B. Krummel, R. L.
Langenfelds, S. O'Doherty, R. G. Prinn, L. P. Steele, M. van der Schoot, and R. F. Weiss, Estimating regional methane
30 surface fluxes: the relative importance of surface and GOSAT mole fraction measurements, Atmos. Chem. Phys., 13, 5697–
5713, 2013 \[www.atmos-chem-phys.net/13/5697/2013/\]\(http://www.atmos-chem-phys.net/13/5697/2013/\) doi:10.5194/acp-13-5697-2013](http://dx.doi.org/10.5194/acp-13-5697-2013)

Gurney, K. R., Law, R. M., Denning, A. S., Rayner, P. J., Baker, D., Bousquet, P., Bruhwiler, L., Chen, Y.-H., Ciais, P., Fan,
S., Fung, I. Y., Gloor, M., Heimann, M., Higuchi, K., John, J., Maki, T., Maksyutov, S., Masarie, K., Peylin, P., Prather, M.,



- Pak, B. C., Randerson, J., Sarmiento, J., Taguchi, S., Takahashi, T., and Yuen, C.-W.: Towards robust regional estimates of CO₂ sources and sinks using atmospheric transport models, *Nature*, 415, 626–630, doi:10.1038/415626a, 2002.
- Griffith, D. W. T., N. Deutscher, V. A. Velazco, P. O. Wennberg, Y. Yavin, G. Keppel Aleks, R. Washenfelder, G. C. Toon,
5 J.-F. Blavier, C. Murphy, N. Jones, G. Kettlewell, B. Connor, R. Macatangay, C. Roehl, M. Ryzek, J. Glowacki, T. Culgan,
G. Bryant. 2014. TCCON data from Darwin, Australia, Release GGG2014R0. TCCON data archive, hosted by the Carbon
Dioxide Information Analysis Center, Oak Ridge National Laboratory, Oak Ridge, Tennessee, U.S.A.
<http://dx.doi.org/10.14291/tcon.ggg2014.darwin01.R0/1149290>
- 10 Griffith, D. W. T., V. A. Velazco, N. Deutscher, C. Murphy, N. Jones, S. Wilson, R. Macatangay, G. Kettlewell, R. R.
Buchholz, M. Riggenbach. 2014. TCCON data from Wollongong, Australia, Release GGG2014R0. TCCON data archive,
hosted by the Carbon Dioxide Information Analysis Center, Oak Ridge National Laboratory, Oak Ridge, Tennessee, U.S.A.
<http://dx.doi.org/10.14291/tcon.ggg2014.wollongong01.R0/1149291>
- 15 Hase, F., T. Blumenstock, S. Dohe, J. Groß, M. Kiel. 2014. TCCON data from Karlsruhe, Germany, Release GGG2014R1.
TCCON data archive, hosted by the Carbon Dioxide Information Analysis Center, Oak Ridge National Laboratory, Oak
Ridge, Tennessee, U.S.A. <http://dx.doi.org/10.14291/tcon.ggg2014.karlsruhe01.R1/1182416>
- Hopkins, F. M., E. A. Kort, S. E. Bush, J. R. Ehleringer, C.-T. Lai, D. R. Blake, and J. T. Randerson (2016), Spatial patterns
20 and source attribution of urban methane in the Los Angeles Basin, *J. Geophys. Res. Atmos.*, 121, 2490–2507,
doi:10.1002/2015JD024429.
- IPCC, 2013: *Climate Change 2013: The Physical Science Basis. Contribution of Working Group I to the Fifth Assessment
Report of the Intergovernmental Panel on Climate Change* [Stocker, T.F., D. Qin, G.-K. Plattner, M. Tignor, S.K. Allen, J.
25 Boschung, A. Nauels, Y. Xia, V. Bex and P.M. Midgley (eds.)]. Cambridge University Press, Cambridge, United Kingdom
and New York, NY, USA, 1535 pp, doi:10.1017/CBO9781107415324.
- Iraci, L., J. Podolske, P. Hillyard, C. Roehl, P. O. Wennberg, J.-F. Blavier, J. Landeros, N. Allen, D. Wunch, J. Zavaleta, E.
Quigley, G. Osterman, E. Barrow, J. Barney. 2014. TCCON data from Indianapolis, Indiana, USA, Release GGG2014R0.
30 TCCON data archive, hosted by the Carbon Dioxide Information Analysis Center, Oak Ridge National Laboratory, Oak
Ridge, Tennessee, U.S.A. <http://dx.doi.org/10.14291/tcon.ggg2014.indianapolis01.R0/1149164>
- Iraci, L., J. Podolske, P. Hillyard, C. Roehl, P. O. Wennberg, J.-F. Blavier, J. Landeros, N. Allen, D. Wunch, J. Zavaleta, E.
Quigley, G. Osterman, R. Albertson, K. Dunwoody, H. Boyden. 2014. TCCON data from Armstrong Flight Research



Center, Edwards, CA, USA, Release GGG2014R0. TCCON data archive, hosted by the Carbon Dioxide Information Analysis Center, Oak Ridge National Laboratory, Oak Ridge, Tennessee, U.S.A.
<http://dx.doi.org/10.14291/tcon.ggg2014.edwards01.R0/1149289>

- 5 Jones, A. K. A. Walker, J. J. Jin, J. R. Taylor, C. D. Boone, P. F. Bernath, S. Brohede, G. L. Manney, S. McLeod, R. Hughes, and W. H. Daffer, Technical Note: A trace gas climatology derived from the Atmospheric Chemistry Experiment Fourier Transform Spectrometer (ACE-FTS) data set, *Atmos. Chem. Phys.*, 12, 5207–5220, 2012, www.atmos-chem-phys.net/12/5207/2012/, doi:10.5194/acp-12-5207-2012
- 10 Kivi, R., P. Heikkinen, E. Kyrö. 2014. TCCON data from Sodankyla, Finland, Release GGG2014R0. TCCON data archive, hosted by the Carbon Dioxide Information Analysis Center, Oak Ridge National Laboratory, Oak Ridge, Tennessee, U.S.A.
<http://dx.doi.org/10.14291/tcon.ggg2014.sodankyla01.R0/1149280>
- Kerridge, B.J. et al PREMIER Consolidation of Requirements and Synergistic Algorithms (CORSA) Study. Final Report,
15 2012. ESA contract 4200022848/09/NL/CT.
- Kirschke, Stefanie et al., Three decades of global methane sources and sinks, *NATURE GEOSCIENCE* | VOL 6 | OCTOBER 2013
- Kort, E. A., C. Frankenberg, K. R. Costigan, R. Lindenmaier, M. K. Dubey, and D. Wunch (2014), Four corners: The largest
20 US methane anomaly viewed from space, *Geophys. Res. Lett.*, 41, 6898–6903, doi:10.1002/2014GL061503
- Kulawik, S. S., J. Worden, A. Eldering, K. Bowman, M. Gunson, G. B. Osterman, L. Zhang, S. A. Clough, M. W. Shephard, and R. Beer (2006), Implementation of cloud retrievals for Tropospheric Emission Spectrometer (TES) atmospheric retrievals: part 1. Description and characterization of errors on trace gas retrievals, *J. Geophys. Res.*, 111, D24204,
25 doi:10.1029/2005JD006733.
- Kuze, Akihiko, Hiroshi Suto, Kei Shiomi, Masakatsu Nakajima, and Takashi Hamazaki, On-orbit performance and level 1 data processing of TANSO-FTS and CAI on GOSAT, *Sensors, Systems, and Next-Generation Satellites XIII*, edited by Roland Meynart, Steven P. Neeck, Haruhisa Shimoda, *Proc. of SPIE Vol. 7474*, 74740I
30
- Kuze, Akihiko Kuze, Hiroshi Suto, Kei Shiomi, Shuji Kawakami, Makoto Tanaka, Yoko Ueda, Akira Deguchi, Jun Yoshida, Yoshifumi Yamamoto, Fumie Kataoka, Thomas E. Taylor, and Henry L. Buijs, Update on GOSAT TANSO-FTS performance, operations, and data products after more than 6 years in space, *Atmos. Meas. Tech.*, 9, 2445–2461, 2016
www.atmos-meas-tech.net/9/2445/2016/ doi:10.5194/amt-9-2445-2016



- Morino, I., N. Yokozeki, T. Matzuzaki, A. Shishime. 2014. TCCON data from Rikubetsu, Hokkaido, Japan, Release GGG2014R0. TCCON data archive, hosted by the Carbon Dioxide Information Analysis Center, Oak Ridge National Laboratory, Oak Ridge, Tennessee, U.S.A. <http://dx.doi.org/10.14291/tcon.ggg2014.rikubetsu01.R0/1149282>
- 5 Morino, I., T. Matsuzaki, A. Shishime. 2014. TCCON data from Tsukuba, Ibaraki, Japan, 125HR, Release GGG2014R0. TCCON data archive, hosted by the Carbon Dioxide Information Analysis Center, Oak Ridge National Laboratory, Oak Ridge, Tennessee, U.S.A. <http://dx.doi.org/10.14291/tcon.ggg2014.tsukuba02.R0/1149301>
- Notholt, J., C. Petri, T. Warneke, N. Deutscher, M. Buschmann, C. Weinzierl, R. Macatangay, P. Grupe. 2014. TCCON data
10 from Bremen, Germany, Release GGG2014R0. TCCON data archive, hosted by the Carbon Dioxide Information Analysis Center, Oak Ridge National Laboratory, Oak Ridge, Tennessee, U.S.A. <http://dx.doi.org/10.14291/tcon.ggg2014.bremen01.R0/1149275>
- Nisbet, Euan G., Edward J. Dlugokencky, Philippe Bousquet, Methane on the Rise again, SCIENCE VOL 343 31
15 JANUARY 2014
- Parker, Robert, Hartmut Boesch, Austin Cogan, Annemarie Fraser, Liang Feng, Paul I. Palmer, Janina Messerschmidt, Nicholas Deutscher, David W. T. Griffith, Justus Notholt, Paul O. Wennberg, and Debra Wunch, Methane observations from the Greenhouse Gases Observing SATellite: Comparison to ground-based TCCON data and model calculations,
20 GEOPHYSICAL RESEARCH LETTERS, VOL. 38, L15807, doi:10.1029/2011GL047871, 2011
- Parker, R. J. Parker, H. Boesch, K. Byckling, A. J. Webb, P. I. Palmer, L. Feng, P. Bergamaschi, F. Chevallier, J. Notholt, N. Deutscher, T. Warneke, F. Hase, R. Sussmann, S. Kawakami, R. Kivi, D. W. T. Griffith, and V. Velasco, Assessing 5 years of GOSAT Proxy XCH₄ data and associated uncertainties, Atmos. Meas. Tech., 8, 4785–4801, 2015, www.atmos-meas-tech.net/8/4785/2015/, doi:10.5194/amt-8-4785-2015
25
- Poulsen, C. A. R. Siddans, G. E. Thomas, A. M. Sayer, R. G. Grainger, E. Campmany, S. M. Dean, C. Arnold, and P. D. Watts, Cloud retrievals from satellite data using optimal estimation: evaluation and application to ATSR, Atmos. Meas. Tech., 5, 1889–1910, 2012, <http://www.atmos-meas-tech.net/5/1889/2012/>, doi:10.5194/amt-5-1889-2012
30
- Razavi, A., C. Clerbaux, C. Wespes, L. Clarisse, D. Hurtmans, S. Payan, C. Camy-Peyret, and P. F. Coheur, Characterization of methane retrievals from the IASI space-borne sounder, Atmos. Chem. Phys., 9, 7889–7899, 2009, www.atmos-chem-phys.net/9/7889/2009/



- Rigby, M., R. G. Prinn, P. J. Fraser, P. G. Simmonds, R. L. Langenfelds, J. Huang, D. M. Cunnold, L. P. Steele, P. B. Krummel, R. F. Weiss, S. O'Doherty, P. K. Salameh, H. J. Wang, C. M. Harth, J. Muhle and L. W. Porter, Renewed growth of atmospheric methane, GEOPHYSICAL RESEARCH LETTERS, VOL. 35, L22805, doi:10.1029/2008GL036037, 2008
- 5
- Sherlock, V., B. Connor, J. Robinson, H. Shiona, D. Smale, D. Pollard. 2014. TCCON data from Lauder, New Zealand, 120HR, Release GGG2014R0. TCCON data archive, hosted by the Carbon Dioxide Information Analysis Center, Oak Ridge National Laboratory, Oak Ridge, Tennessee, U.S.A. <http://dx.doi.org/10.14291/tcon.ggg2014.lauder01.R0/1149293>
- 10
- Sherlock, V., B. Connor, J. Robinson, H. Shiona, D. Smale, D. Pollard. 2014. TCCON data from Lauder, New Zealand, 125HR, Release GGG2014R0. TCCON data archive, hosted by the Carbon Dioxide Information Analysis Center, Oak Ridge National Laboratory, Oak Ridge, Tennessee, U.S.A. <http://dx.doi.org/10.14291/tcon.ggg2014.lauder02.R0/1149298>
- Shiomi, K., Kawakami, S., H. Ohyama, K. Arai, H. Okumura, C. Taura, T. Fukamachi, M. Sakashita. 2014. TCCON data from Saga, Japan, Release GGG2014R0. TCCON data archive, hosted by the Carbon Dioxide Information Analysis Center, Oak Ridge National Laboratory, Oak Ridge, Tennessee, U.S.A. <http://dx.doi.org/10.14291/tcon.ggg2014.saga01.R0/1149283>
- 15
- Strong, K., J. Mendonca, D. Weaver, P. Fogal, J.R. Drummond, R. Batchelor, R. Lindenmaier. 2014. TCCON data from Eureka, Canada, Release GGG2014R0. TCCON data archive, hosted by the Carbon Dioxide Information Analysis Center, Oak Ridge National Laboratory, Oak Ridge, Tennessee, U.S.A. <http://dx.doi.org/10.14291/tcon.ggg2014.eureka01.R0/1149271>
- 20
- Sussmann, R., M. Rettinger. 2014. TCCON data from Garmisch, Germany, Release GGG2014R0. TCCON data archive, hosted by the Carbon Dioxide Information Analysis Center, Oak Ridge National Laboratory, Oak Ridge, Tennessee, U.S.A. <http://dx.doi.org/10.14291/tcon.ggg2014.garmisch01.R0/1149299>
- 25
- Sussman, R., F. Forster, M. Rettinger, and P. Bousquet, Renewed methane increase for five years (2007–2011) observed by solar FTIR spectrometry, Atmos. Chem. Phys., 12, 4885–4891, 2012 www.atmos-chem-phys.net/12/4885/2012/, doi:10.5194/acp-12-4885-2012
- 30
- Te, Y., P. Jeseck, C. Janssen. 2014. TCCON data from Paris, France, Release GGG2014R0. TCCON data archive, hosted by the Carbon Dioxide Information Analysis Center, Oak Ridge National Laboratory, Oak Ridge, Tennessee, U.S.A. <http://dx.doi.org/10.14291/tcon.ggg2014.paris01.R0/1149279>



von Clarmann, T., Smoothing error pitfalls, Atmos. Meas. Tech., 7, 3023–3034, 2014, www.atmos-meas-tech.net/7/3023/2014/, doi:10.5194/amt-7-3023-2014

Warneke, T., J. Messerschmidt, J. Notholt, C. Weinzierl, N. Deutscher, C. Petri, P. Grupe, C. Vuillemin, F. Truong, M. Schmidt, M. Ramonet, E. Parmentier. 2014. TCCON data from Orleans, France, Release GGG2014R0. TCCON data
5 archive, hosted by the Carbon Dioxide Information Analysis Center, Oak Ridge National Laboratory, Oak Ridge, Tennessee, U.S.A. <http://dx.doi.org/10.14291/tcon.ggg2014.orleans01.R0/1149276>

Wecht, K. J., D. J. Jacob, S. C. Wofsy, E. A. Kort, J. R. Worden, S. S. Kulawik, D. K. Henze, M. Kopacz, and V. H. Payne
10 (2012), Validation of TES methane with HIPPO aircraft observations: implications for inverse modeling of methane sources, Atmospheric Chemistry and Physics, 12(4), 1823–1832, doi:10.5194/acp-12-1823-2012.

Wennberg, P. O., C. Roehl, D. Wunch, G. C. Toon, J.-F. Blavier, R. Washenfelder, G. Keppel-Aleks, N. Allen, J. Ayers.
15 2014. TCCON data from Park Falls, Wisconsin, USA, Release GGG2014R0. TCCON data archive, hosted by the Carbon Dioxide Information Analysis Center, Oak Ridge National Laboratory, Oak Ridge, Tennessee, U.S.A. <http://dx.doi.org/10.14291/tcon.ggg2014.parkfalls01.R0/1149161>

Wennberg, P. O., C. Roehl, J.-F. Blavier, D. Wunch, J. Landeros, N. Allen. 2014. TCCON data from Jet Propulsion
20 Laboratory, Pasadena, California, USA, Release GGG2014R0. TCCON data archive, hosted by the Carbon Dioxide Information Analysis Center, Oak Ridge National Laboratory, Oak Ridge, Tennessee, U.S.A. <http://dx.doi.org/10.14291/tcon.ggg2014.jpl02.R0/1149297>

Wennberg, P. O., D. Wunch, C. Roehl, J.-F. Blavier, G. C. Toon, N. Allen. 2014. TCCON data from California Institute of
25 Technology, Pasadena, California, USA, Release GGG2014R1. TCCON data archive, hosted by the Carbon Dioxide Information Analysis Center, Oak Ridge National Laboratory, Oak Ridge, Tennessee, U.S.A. <http://dx.doi.org/10.14291/tcon.ggg2014.pasadena01.R1/1182415>

Wennberg, P. O., D. Wunch, C. Roehl, J.-F. Blavier, G. C. Toon, N. Allen, P. Dowell, K. Teske, C. Martin, J. Martin. 2014.
30 TCCON data from Lamont, Oklahoma, USA, Release GGG2014R0. TCCON data archive, hosted by the Carbon Dioxide Information Analysis Center, Oak Ridge National Laboratory, Oak Ridge, Tennessee, U.S.A. <http://dx.doi.org/10.14291/tcon.ggg2014.lamont01.R0/1149159>

Wennberg, P. O., D. Wunch, Y. Yavin, G. C. Toon, J.-F. Blavier, N. Allen, G. Keppel-Aleks. 2014. TCCON data from Jet
Propulsion Laboratory, Pasadena, California, USA, Release GGG2014R0. TCCON data archive, hosted by the Carbon



Dioxide Information Analysis Center, Oak Ridge National Laboratory, Oak Ridge, Tennessee, U.S.A.
<http://dx.doi.org/10.14291/tcon.ggg2014.jpl01.R0/1149163>

- Westbrook, Graham K., Thatcher, Kate E., Rohling, Eelco J., Piotrowski, Alexander M., Pälke, Heiko, Osborne, Anne H.,
5 Nisbet, Euan G., Minshull, Tim A., Lanoisellé, Mathias, James, Rachael H., Huhnerbach, Veit, Green, Darryl, Fisher,
Rebecca E., Crocker, Anya J., Chabert, Anne, Bolton, Clara, Beszczynska-Möller, Agnieszka, Berndt, Christian and
Aquilina, Alfred (2009) Escape of methane gas from the seabed along the West Spitsbergen continental margin. *Geophysical
Research Letters*, 36, L15608. (doi:10.1029/2009GL039191).
- 10 Wofsy, S. C., B. C. Daube, R. Jimenez, E. Kort, J. V. Pittman, S. Park, R. Commane, B. Xiang, G. Santoni, D. Jacob, J.
Fisher, C. Pickett-Heaps, H. Wang, K. Wecht, Q.-Q. Wang, B. B. Stephens, S. Shertz, A.S. Watt, P. Romashkin, T. Campos,
J. Haggerty, W. A. Cooper, D. Rogers, S. Beaton, R. Hendershot, J. W. Elkins, D. W. Fahey, R. S. Gao, F. Moore, S. A.
Montzka, J. P. Schwarz, A. E. Perring, D. Hurst, B. R. Miller, C. Sweeney, S. Oltmans, D. Nance, E. Hints, G. Dutton, L.
A. Watts, J. R. Spackman, K. H. Rosenlof, E. A. Ray, B. Hall, M. A. Zondlo, M. Diao, R. Keeling, J. Bent, E. L. Atlas, R.
15 Lueb, M. J. Mahoney. 2012. HIPPO Merged 10-second Meteorology, Atmospheric Chemistry, Aerosol Data (R_20121129).
Carbon Dioxide Information Analysis Center, Oak Ridge National Laboratory, Oak Ridge, Tennessee, U.S.A.
http://dx.doi.org/10.3334/CDIAC/hippo_010 (Release 20121129)
- Worden, J., S. Kulawik, C. Frankenberg, V. Payne, K. Bowman, K. Cady-Peirara, K. Wecht, J.-E. Lee, and D. Noone,
20 Profiles of CH₄, HDO, H₂O, and N₂O with improved lower tropospheric vertical resolution from Aura TES radiances,
Atmos. Meas. Tech., 5, 397–411, 2012, www.atmos-meas-tech.net/5/397/2012/, doi:10.5194/amt-5-397-2012
Worden, J., K. Wecht, C. Frankenberg, M. Alvarado, K. Bowman, E. Kort, S. Kulawik, M. Lee, V. Payne, and H. Worden,
CH₄ and CO distributions over tropical fires during October 2006 as observed by the Aura TES satellite instrument and
modeled by GEOS-Chem, *Atmos. Chem. Phys.*, 13, 3679–3692, 2013, www.atmos-chem-phys.net/13/3679/2013/,
25 doi:10.5194/acp-13-3679-2013
- Worden, J.R., A. J. Turner, A. Bloom, S. S. Kulawik, J. Liu, M. Lee, R. Weidner, K. Bowman, C. Frankenberg, R. Parker,
and V. H. Payne, Quantifying lower tropospheric methane concentrations using GOSAT near-IR and TES thermal IR
measurements, *Atmos. Meas. Tech.*, 8, 3433–3445, 2015, www.atmos-meas-tech.net/8/3433/2015/, doi:10.5194/amt-8-3433-
30 2015
- Wunch, D., G.C. Toon, J.-F.L. Blavier, R.A. Washenfelder, J. Notholt, B.J. Connor, D.W.T. Griffith, V. Sherlock, P.O.
Wennberg. The Total Carbon Column Observing Network. *Phil. Trans. R. Soc. A* (2011) 369, doi:10.1098/rsta.2010.0240



Xiong , Xiaozhen, Chris Barnet, Eric Maddy, Colm Sweeney, Xingpin Liu,, Lihang Zhou, and Mitch Goldberg, Characterization and validation of methane products from the Atmospheric Infrared Sounder (AIRS), JOURNAL OF GEOPHYSICAL RESEARCH, VOL. 113, G00A01, doi:10.1029/2007JG000500, 2008

- 5 Xiong, X., C. Barnet, E. S. Maddy, A. Gambacorta, T. S. King, and S. C. Wofsy, Mid-upper tropospheric methane retrieval from IASI and its validation, Atmos. Meas. Tech., 6, 2255–2265, 2013, www.atmos-meas-tech.net/6/2255/2013/, doi:10.5194/amt-6-2255-2013

- Yoshida, Y, N. Kikuchi, I. Morino, O. Uchino, S. Oshchepkov, A. Bril, T. Saeki, N. Schutgens, G. C. Toon, D. Wunch, C.
10 M. Roehl, P. O. Wennberg, D. W. T. Griffith, N. M. Deutscher, T. Warneke, J. Notholt, J. Robinson, V. Sherlock, B. Connor, M. Rettinger, R. Sussmann, P. Ahonen, P. Heikkinen, E. Kyro, J. Mendonca, K. Strong, F. Hase, S. Dohe, and T. Yokota, Improvement of the retrieval algorithm for GOSAT SWIR XCO₂ and XCH₄ and their validation using TCCON data, Atmos. Meas. Tech., 6, 1533–1547, 2013, www.atmos-meas-tech.net/6/1533/2013/, doi:10.5194/amt-6-1533-2013

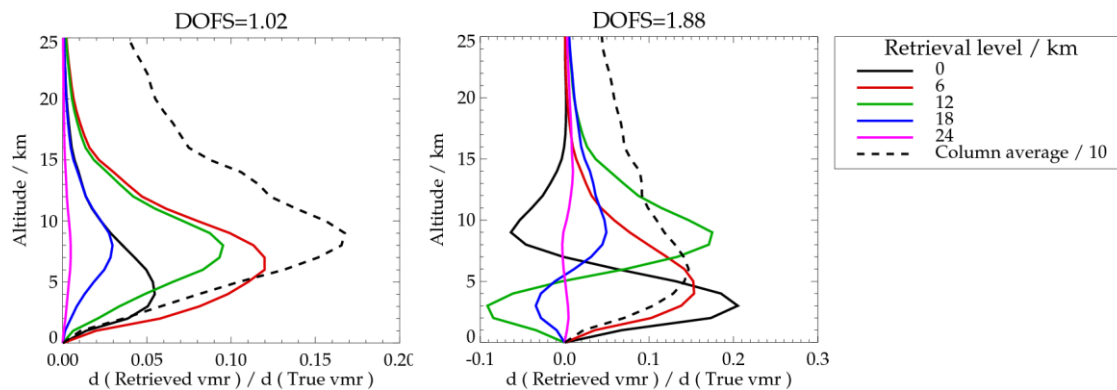


Figure 1: Averaging kernels for the methane profile at each retrieval level (solid) and for the column average (dashed). Panel
5 on left shows result for NEBT=0.5K, on right case for NEBT=0.1L. DOFS of each case is indicated above the panel.

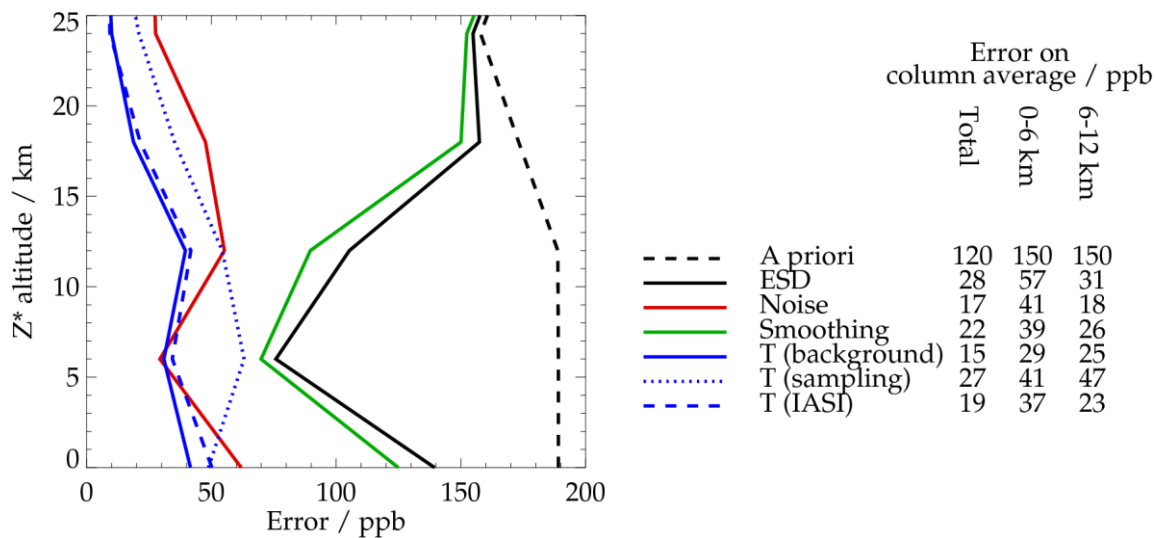


Figure 2: Estimated errors for methane profile (in panel) and column average (indicated in caption).

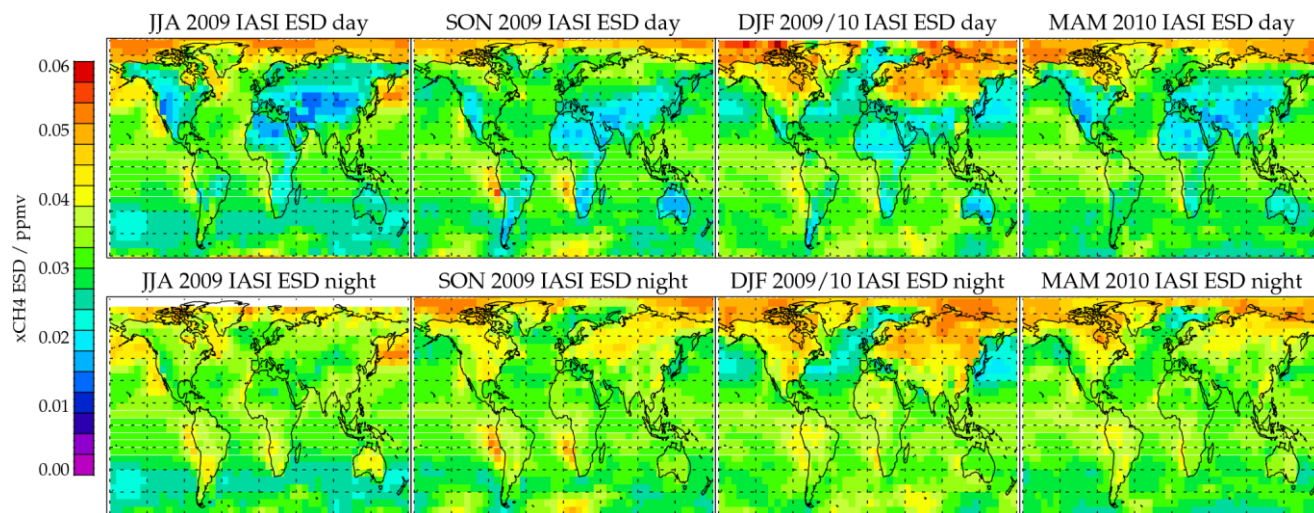
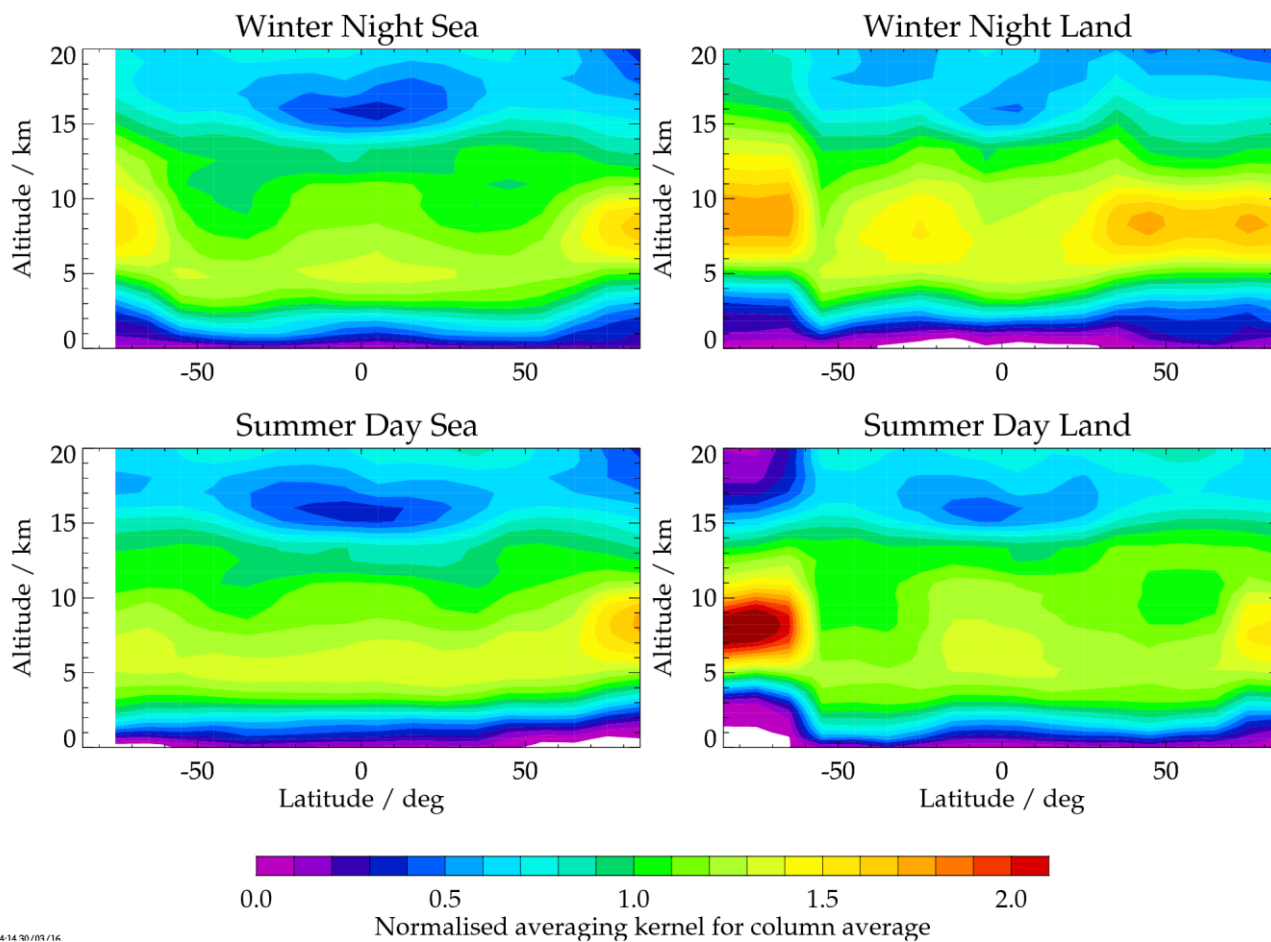


Figure 3: Average in 7.5 x 5 degree latitude/longitude bins of the ESD on the column average mixing ratio as a function of season (left to right) and for day (top) and night-time observing conditions (bottom row). “JJA” = June, July August 2009;
5 “SON” = September, October November 2009; “DJF” = December, January, February 2009/10; “MAM” = March, April, May 2010



1414/20/05/16

Figure 4: Averaging kernels for column averaged methane as a function of latitude and season, for observations over sea, daytime land and night-time land.

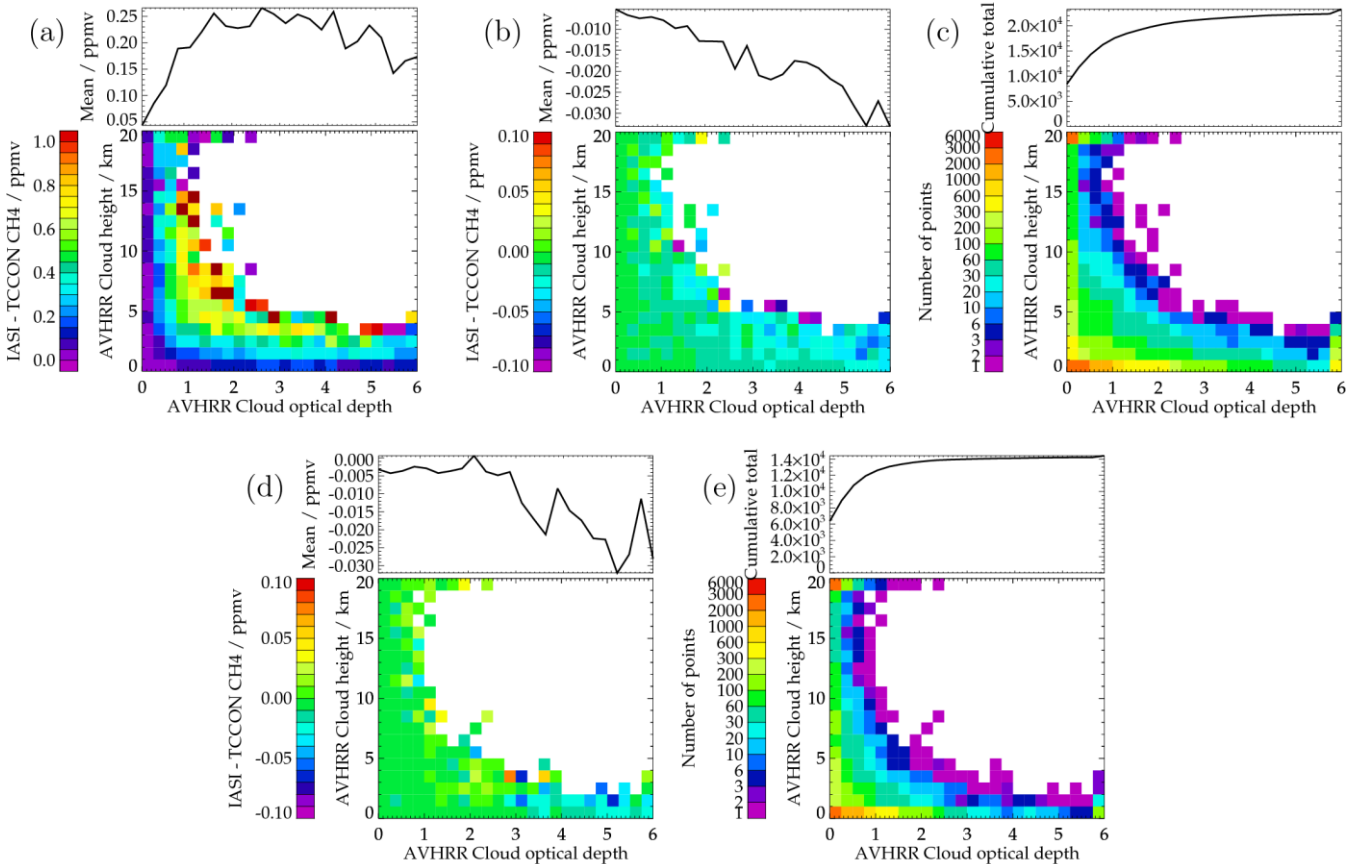


Figure 5: Panel (a) shows the mean differences between IASI and TCCON measurements (in 2009) as a function of the AVHRR cloud optical depth and height, for the retrieval in which N₂O is fitted and cloud neglected. The line plot above shows the mean difference over all cloud heights, as function of optical depth. Panel (b) shows the same but for the new scheme with N₂O defined and cloud parameters retrieved (note the change in ranges shown). Panel (c) shows the number of IASI retrievals in each bin, with the sub-panel above showing the cumulative total number of points as function of increasing optical depth. Panels (d) and (e) show results as panels (c) and (d), respectively, after removing scenes with retrieved cloud fraction larger than 0.2.

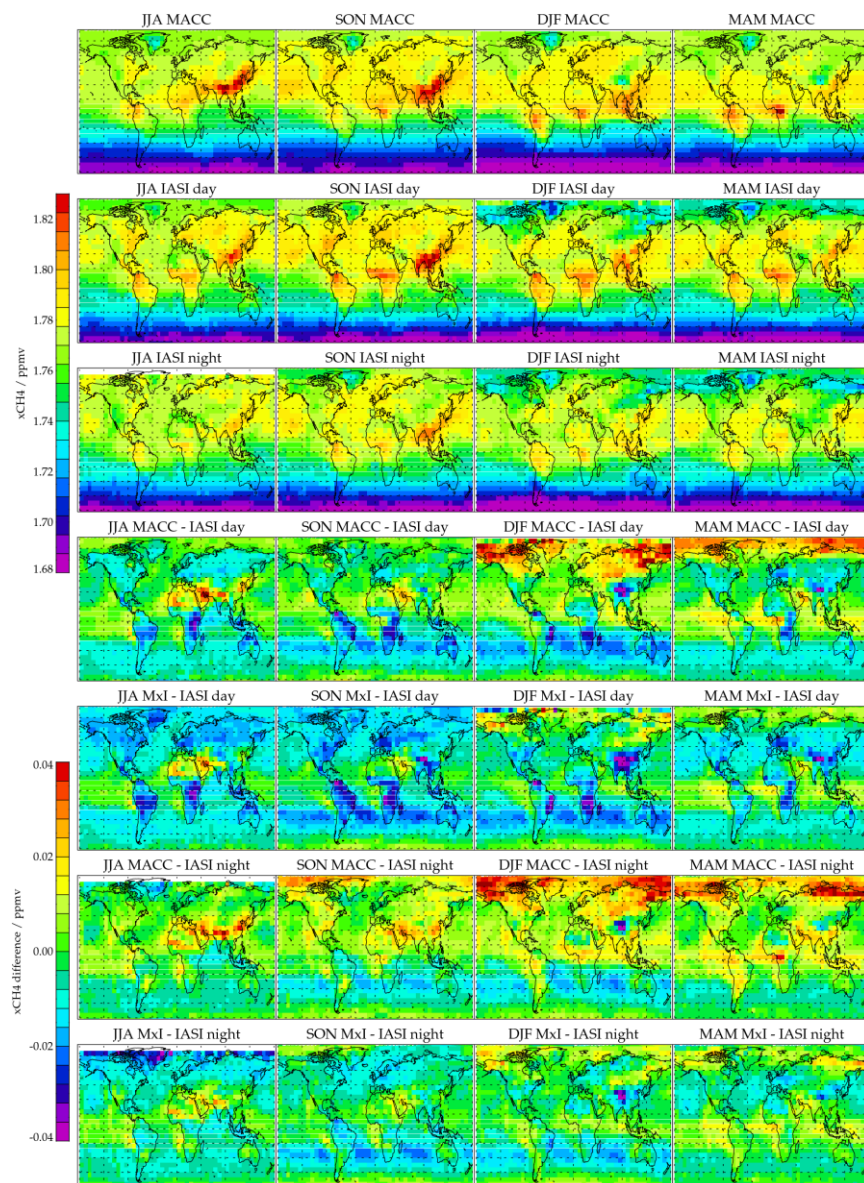


Figure 6: Comparisons of IASI and MACC-II GHG column average mixing ratio. Each column of the figure shows results for a different season; “JJA” = June, July August 2009; “SON” = September, October November 2009; “DJF” = December, January, February 2009/10; “MAM” = March, April, May 2010. The top three rows show, respectively, results from MACC-II GHG, IASI daytime retrievals and IASI night-time retrievals. Bottom rows show differences between MACC-II GHG and IASI, separately for day and night, with and without taking into account the IASI averaging kernels. “MxI” is used in the panel titles as short-hand for “MACC-II GHG after accounting for IASI averaging kernels”.

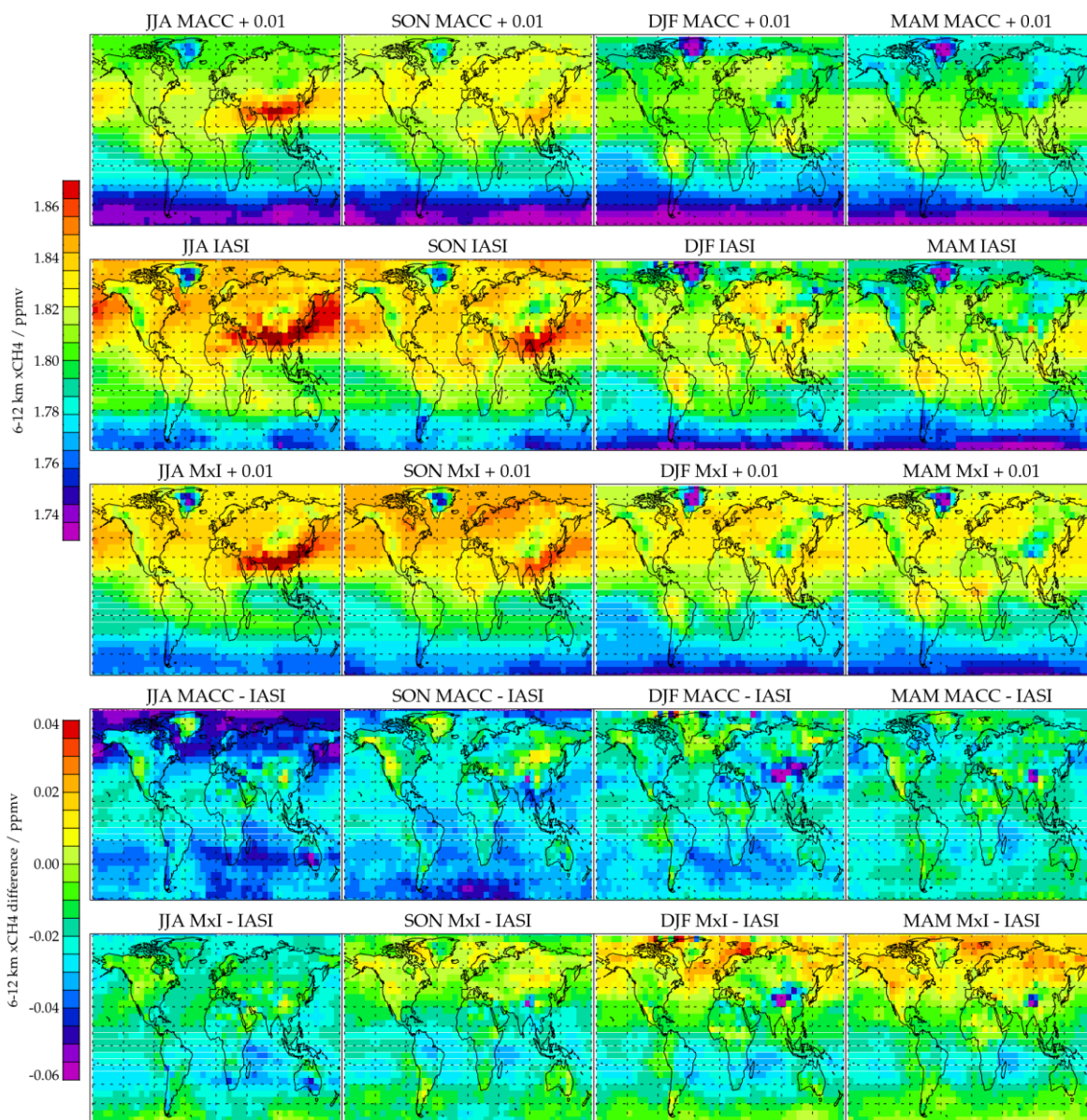


Figure 7: Comparisons of IASI and MACC-II GHG 6-12 km (z^*) sub-column average mixing ratio. Daytime only results shown. The top three rows show, respectively, results from MACC-II GHG, IASI and MACC-II GHG with the IASI averaging kernels applied (“MxI”). MACC and MxI results have 0.01 ppmv added, as indicated in the plot title. Bottom two rows show differences between MACC and IASI directly and after taking into account the IASI averaging kernels (without any offset applied to MACC or MxI).

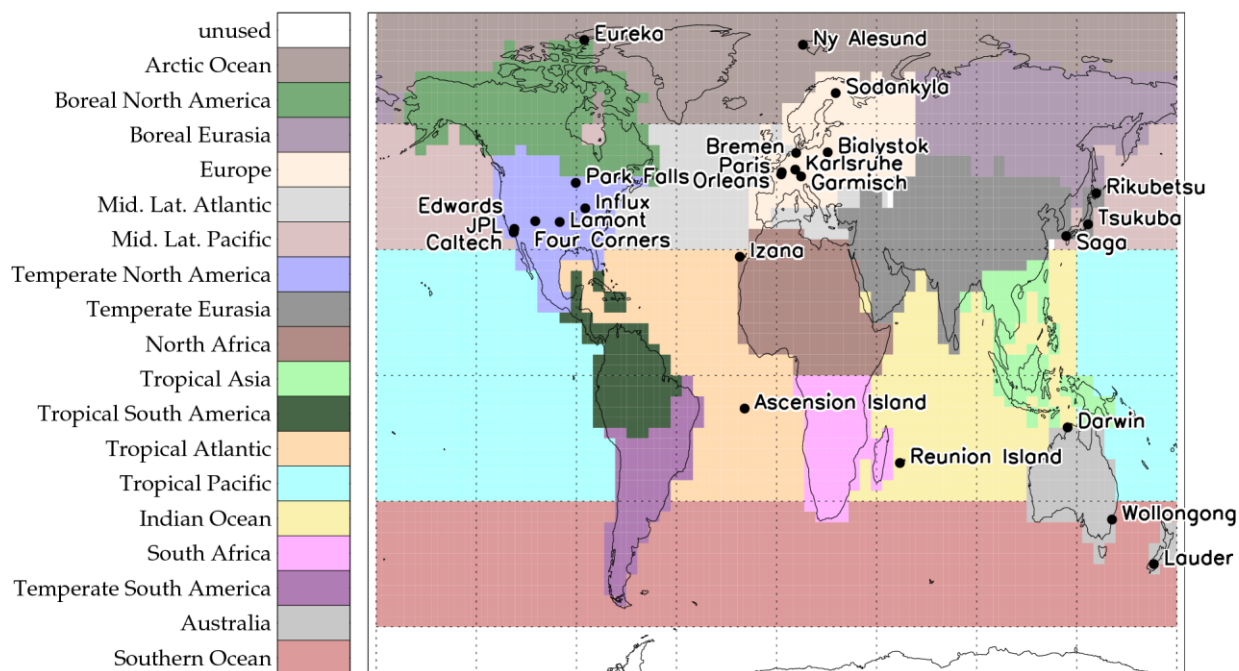


Figure 8: The regions used for comparisons with MACC and the locations of TCCON sites.

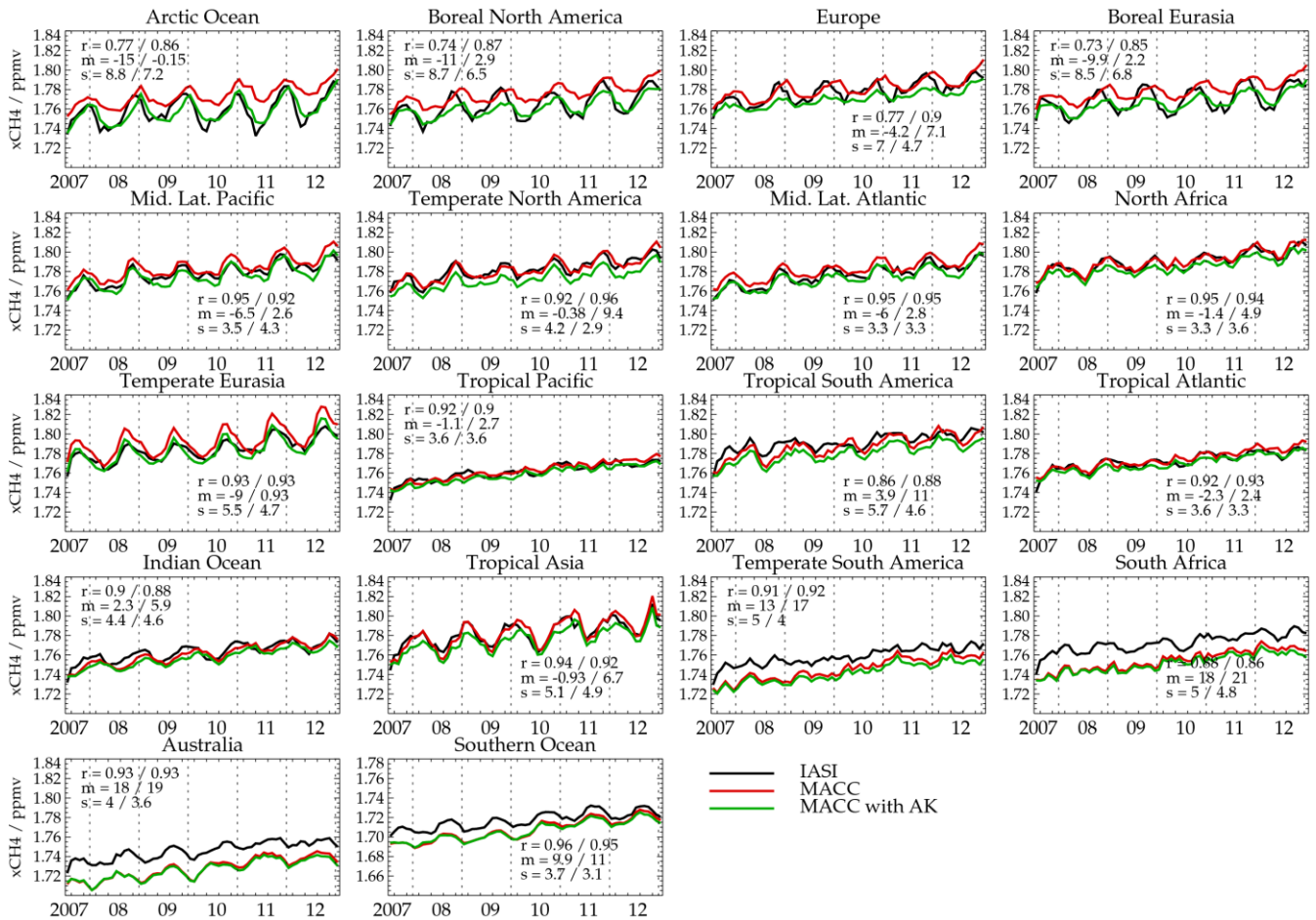


Figure 9: Time series of monthly, regionally averaged total column methane from IASI and MACC. IASI measurements are shown in black; values directly from MACC are in red; MACC results accounting for the IASI averaging kernel are shown in green. The caption in each panel indicates the correlation between IASI and MACC (“r”), the mean difference IASI – MACC (“m”) in ppb and the standard deviation in the difference (“s”) in ppb. Two values are given in each case, first for the direct IASI-MACC comparison, then that accounting for the kernels. Dashed vertical lines mark the beginning and end of each year.

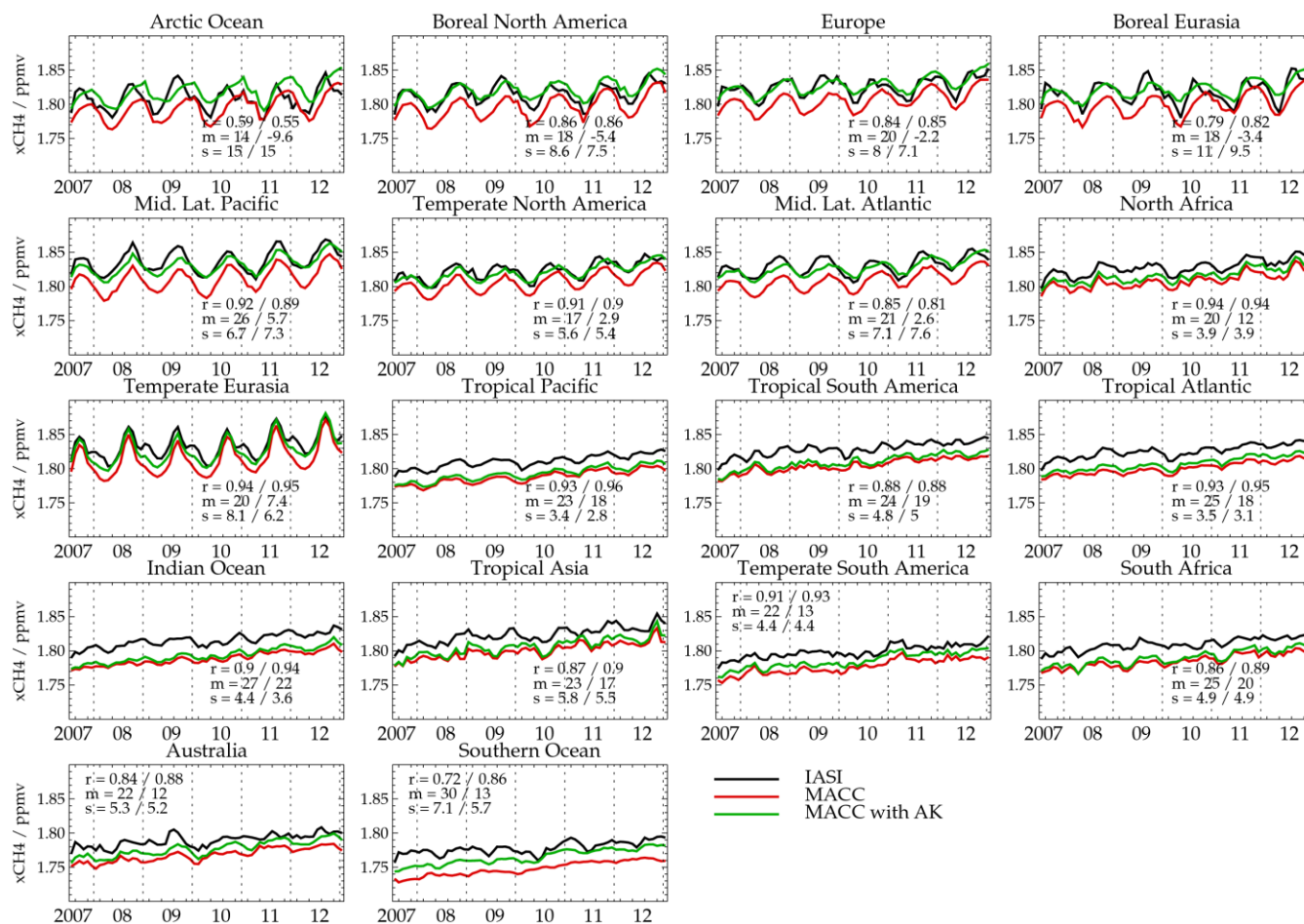


Figure 10: As previous figure, for 6-12 km column average methane.

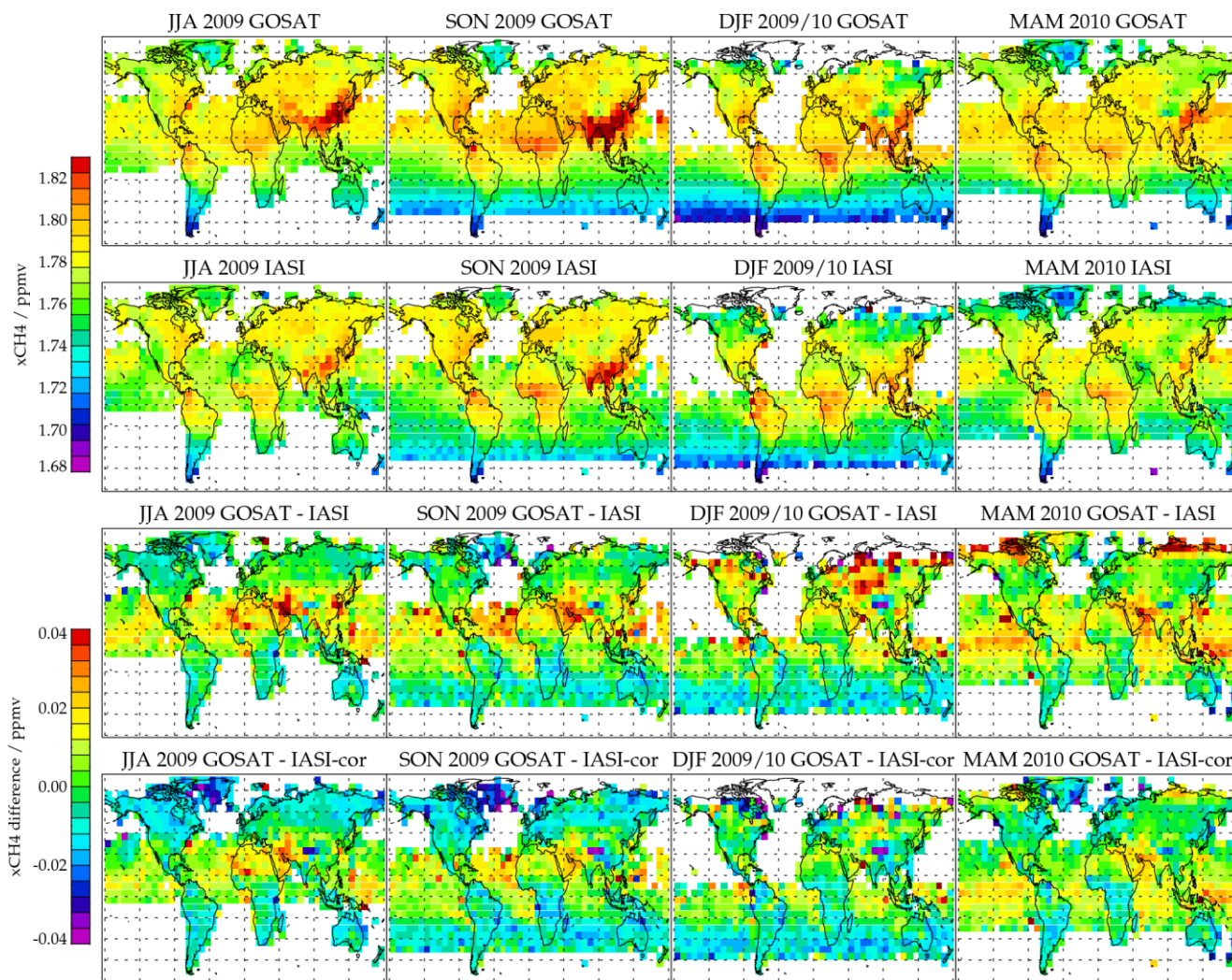


Figure 11: Seasonal mean distributions of total column averaged methane in 2009-10 from GOSAT (top row) and IASI
5 daytime observations, sampled on a daily basis like GOSAT (2nd row). The 4th row shows differences between the GOSAT
and the IASI daytime means. The bottom row shows differences after correcting IASI for differences in the IASI/GOSAT
vertical sensitivity using MACC.

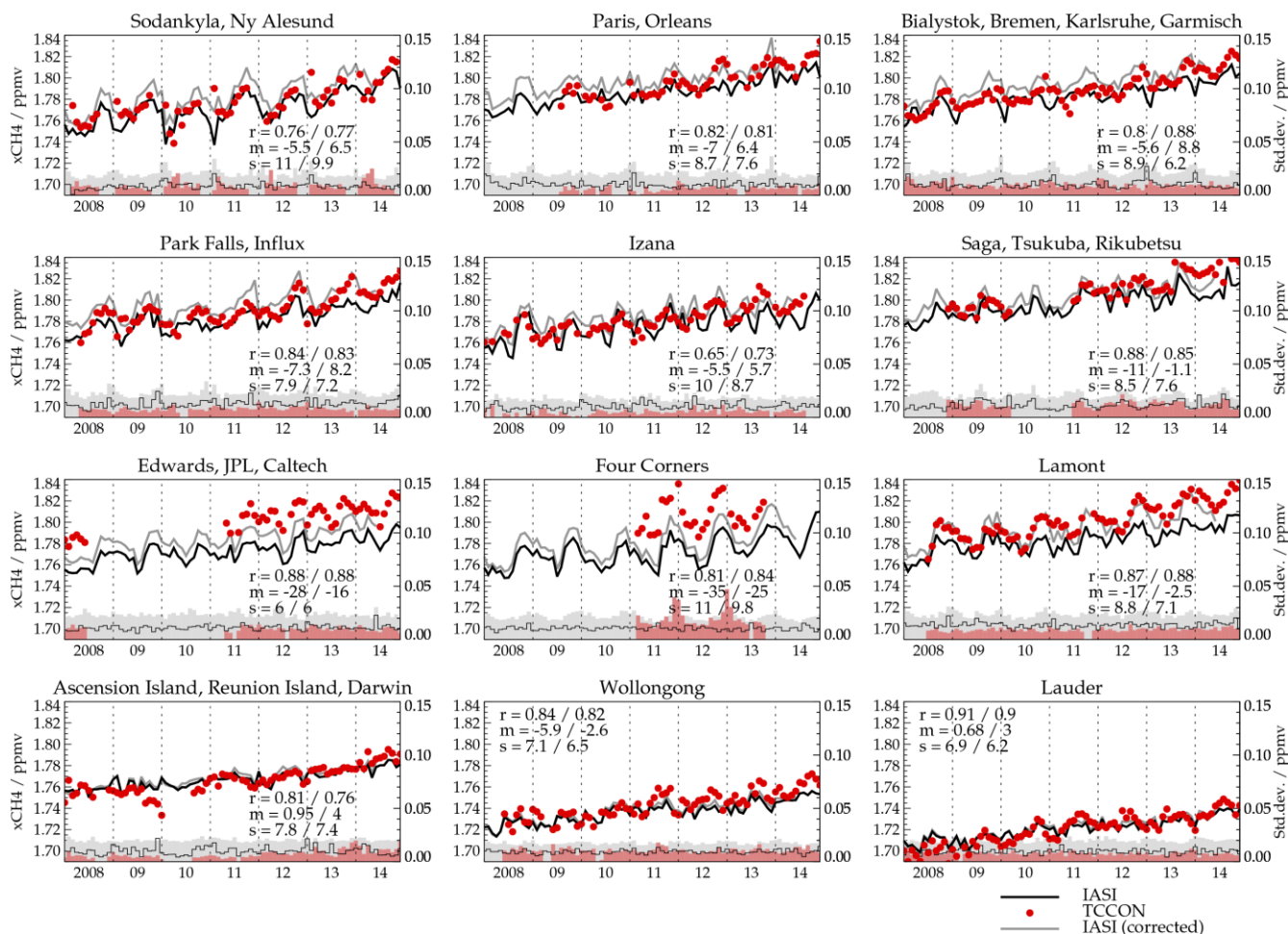


Figure 12: Comparison of IASI and TCCON monthly column averaged methane mixing ratio from 2008-2014. The black line shows IASI and red points show TCCON. The grey line shows the IASI result corrected to account for the IASI smoothing error using MACC (see text). Histograms indicate the standard deviation in the IASI and TCCON monthly mean (refer to right-hand axis). Figures in the caption indicate the correlation coefficient (r), mean difference (“m”, in ppb) and standard deviation in the difference (“s”, in ppb). Two values are given for each quantity (separated by ‘/’), corresponding to the black (IASI direct) and grey (IASI corrected) curves, respectively.

10

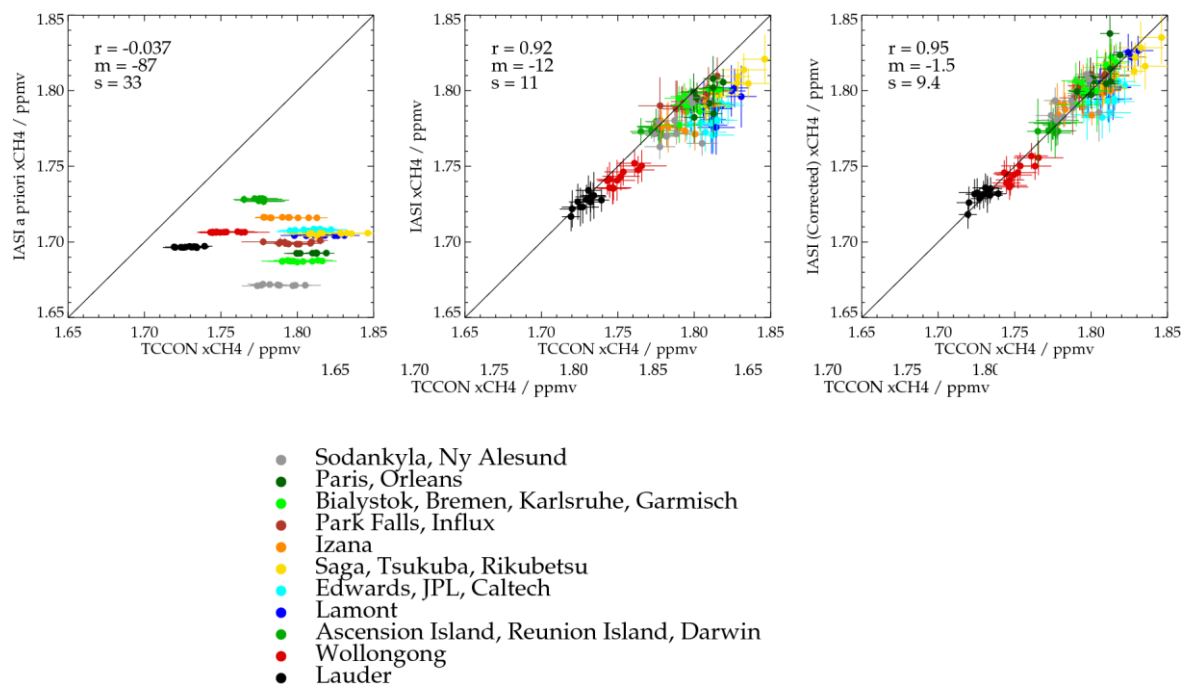


Figure 13: Scatter plots comparing TCCON and IASI column averaged methane mixing ratio in 2013. Each point compares the mean values for each month, with different colours indicated different (groups of) TCCON stations as in the caption. Error bars show the standard deviations in daily mean values within each month. Panels show (from left to right): IASI a priori vs TCCON; IASI vs TCCON; IASI after correction for smoothing error using MACC.

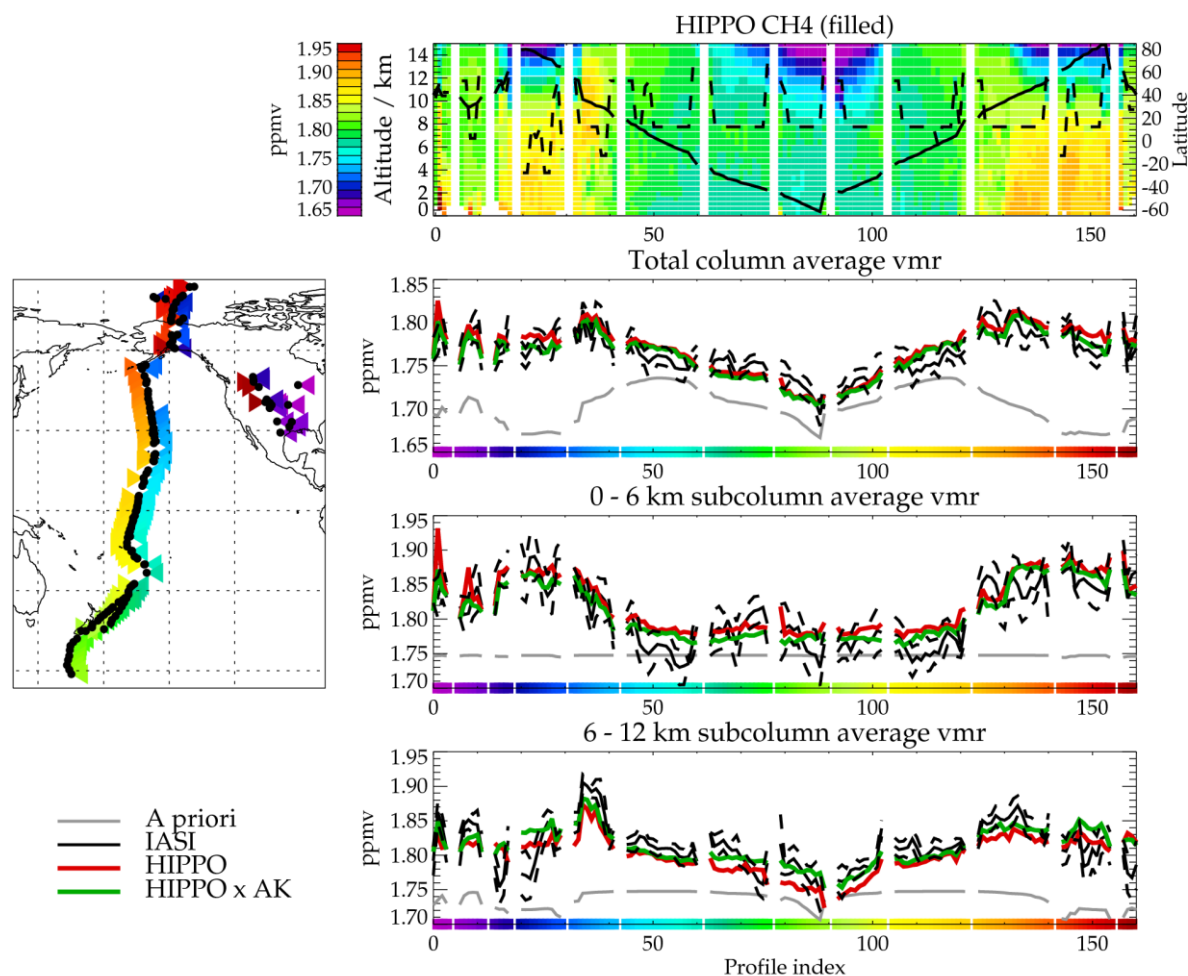


Figure 14: Comparison of IASI and HIPPO for flight campaign 5 (between 9 August and 9 September 2011). Map on the left shows the flight track. Actual measurement locations are indicated with black dots; associated coloured triangles indicate the profile index, as shown on the x-axis of panels on the right (colours under the axis correspond to colours used in the map). The top-right panel shows the cross-section as measured by HIPPO, after binning and filling (upwards) using the MACC GHG reanalysis. The solid black line in this plot shows the latitude of each profile (refer to y-axis on the right); The dashed black line shows the maximum (z^*) altitude of the HIPPO measurement, above which profiles are filled with MACC. Gaps (filled with white) between the coloured regions divide data from different flights (on different days). Panels below compare IASI and HIPPO (sub-)column averaged mixing ratios. The mean of matched IASI retrievals is shown in black. The dashed lines show the mean \pm standard deviation of the matched retrievals. Grey shows the IASI a priori. Red shows the HIPPO result; Green shows HIPPO after taking into account the IASI averaging kernel.

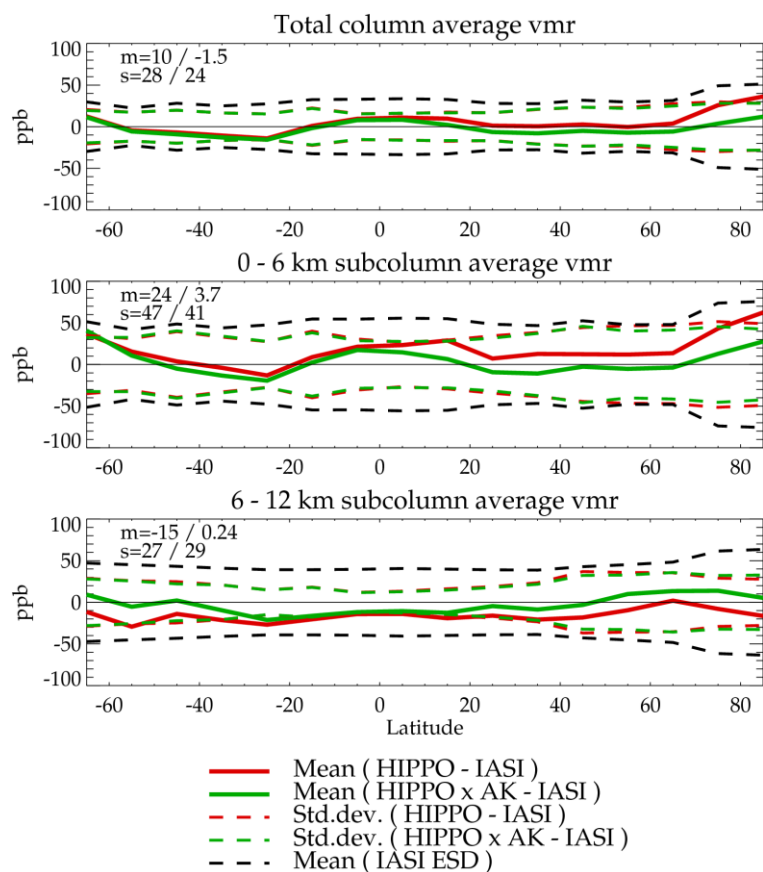


Figure 15: Summary of the differences between IASI and HIPPO for all five HIPPO campaigns. Results are presented averaged into 10 degree latitude bins. As indicated in the legend, solid lines show the mean difference between IASI and HIPPO (with (green) and without (red) IASI averaging kernels being applied to HIPPO data). Corresponding dashed lines show the standard deviation of the individual IASI/HIPPO matches about the mean difference. Black dashed lines show the mean of the IASI ESD on individual soundings. Figures in the top-left of each panel show the mean difference (m) over all matches and the standard-deviation of the individual matches about the mean with / without application of IASI averaging kernels to HIPPO data.